REGIONAL INVESTIGATION OF RARE EARTH ELEMENT-ENRICHED UNDERCLAY DEPOSITS IN THE CENTRAL AND EASTERN UNITED STATES

Report of Investigations No. 37

BY: JESSICA MOORE, HEATHER HANNA, BETHANY ROYCE, GARY DAFT JR., WILLIAM ANDREWS, CORTLAND EBLE, AND SARAH BROWN

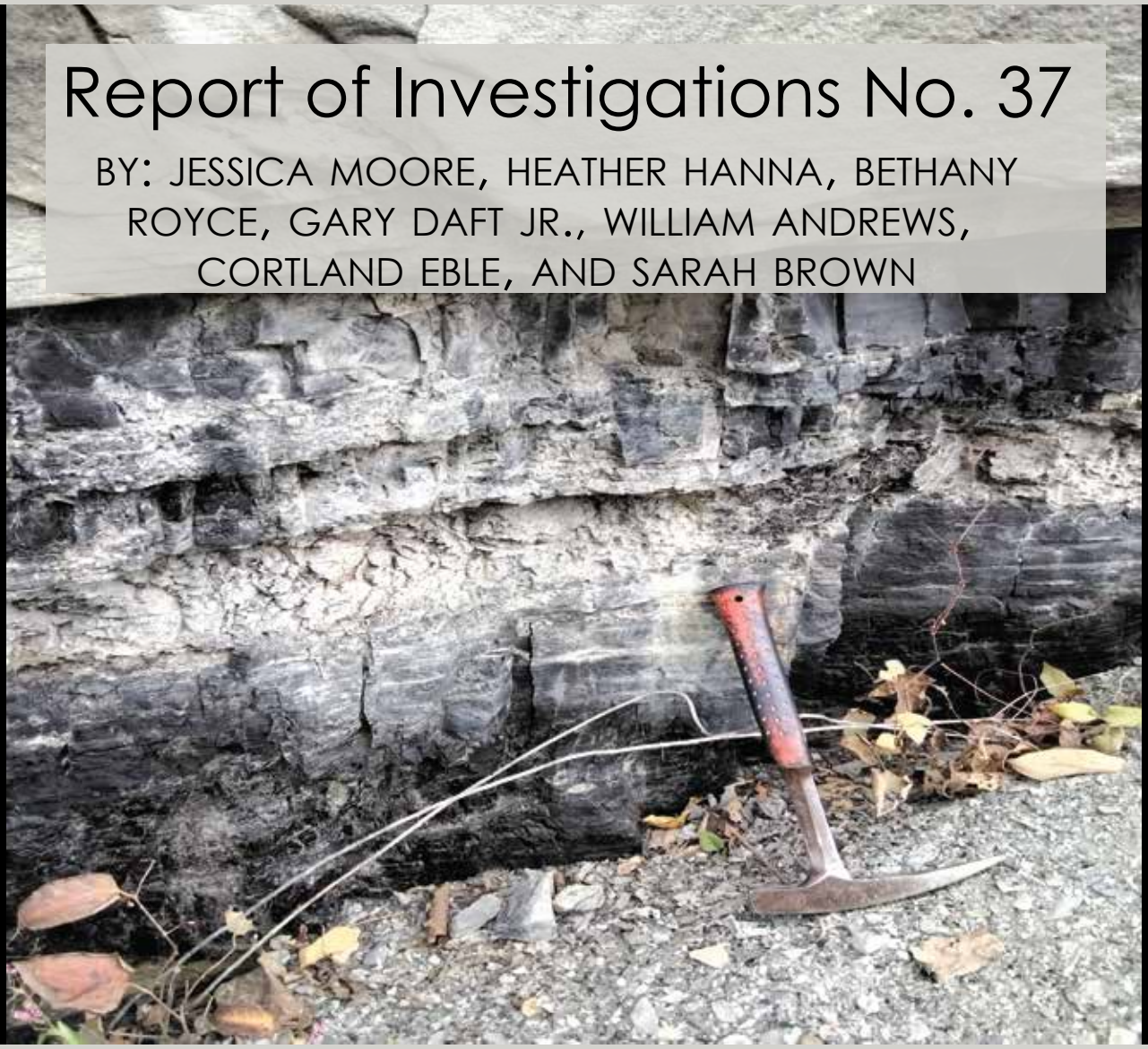

STATE OF WEST VIRGINIA - JIM JUSTICE, GOVERNOR

GEOLOGICAL and ECONOMIC SURVEY

JESSICA MOORE, STATE GEOLOGIST 2024 MORGANTOWN, WEST VIRGINIA

West Virginia Geological & Economic Survey
Reports of Investigation 37

Regional Investigation of Rare Earth Element-Enriched Underclay Deposits in the Central and Eastern United States: an Earth Mapping Resources Initiative (Earth MRI) Geochemical Reconnaissance Study

Jessica Moore[1], Heather Hanna[2], Bethany Royce[1], Gary Daft[1], William Andrews[3], Cortland Eble[3], and Sarah Brown[1]

With Contributions From:

Philip Dinterman[1], Georgina Lukoczki[3], Rebecca Kavage-Adams[4], David Brezinski[4], Kristen Hand[5], Steven Shank[5], Aaron Bierly[5], Frank Fugitt[6], J.D. Stucker[6], Maria Mastalerz[7], Patrick McLaughlin[8], Scott Elrick[8], Jared Freiberg[8], Ryan Clark[9], and Stephanie Tassier-Surine[9]

[1]West Virginia Geological and Economic Survey; [2] Hanna Forensics LLC;
[3]Kentucky Geological Survey; [4]Maryland Geological Survey; [5]Pennsylvania Geological Survey; [6]Ohio Geological Survey; [7]Indiana Geological and Water Survey;
[8]Illinois State Geological Survey; [9]Iowa Geological Survey

Suggested Citation:

Moore, J., Hanna, H., Royce, B., Daft, G., Andrews, W., Eble, C., and Brown, S., 2024, Regional investigation of rare earth element-enriched underclay deposits of the central and eastern United States: An Earth Mapping Resources Initiative (Earth MRI) geochemical reconnaissance study. West Virginia Geological and Economic Survey Reports of Investigation 37. 31pp.

Table of Contents

List of Figures

List of Tables

Chemical Symbols

Abbreviation	Description
Al	Aluminum
Al_2O_3	Aluminum Oxide
Ba	Barium
Bi	Bismuth
CaO	Calcium Oxide
Ce	Cerium
Cr	Chromium
Cu	Copper
Dy	Dysprosium
Er	Erbium
Eu	Europium
Fe	Iron
Fe_2O_3	Iron Oxide
Ga	Gallium
Gd	Gadolinium
Hf	Hafnium
Ho	Holmium
In	Indium
K	Potassium
K_2O	Potassium Oxide
La	Lanthanum
Li	Lithium
Lu	Lutetium
Na_2O	Sodium Oxide
Nb	Niobium
Nd	Neodymium
Ni	Nickel
P	Phosphorus
Pb	Lead
Pr	Praseodymium
Sb	Antimony
Sc	Scandium
SiO_2	Silicon Dioxide
Sm	Samarium
Sr	Strontium
Tb	Terbium
Th	Thorium
Ti	Titanium
Tm	Thulium
U	Uranium
V	Vanadium
Y	Yttrium
Yb	Ytterbium

Zr	Zirconium

List of Symbols, Abbreviations, and Acronyms

(*symbols listed first followed by Greek letter abbreviations followed by other abbreviations and acronyms in alphabetical order*)

Abbreviation	Description
&	and
~	approximately
º	degrees
‘	feet
+	plus; greater; more
-	minus; to
x	times
/	divided by; per; and; or
=	equals
>	greater than
<	less than
#	number
%	percent
C	Celsius
CIA	Chemical Index of Alteration
EMRI or Earth MRI	Earth Mapping Resources Imitative
g	Grams
HREE	Heavy Rare Earth Elements
hhXRF	Handheld X-Ray Fluorescence
ICP-OES/ICP-MS	Inductively Coupled Plasma-Optical Emission Spectroscopy-Mass Spectroscopy
IOL	Index of Laterization
KGS	Kentucky Geological Survey
kV	Kilovolt
LOD	Limits of Detection
LREE	Light Rare Earth Elements
mA	Milliamps
MD	Maryland
MDS	Multidimensional space
ml	Milliliters
mm	Millimeters
MREE	Middle Rare Earth Elements
Mya	Million years ago
NETL	National Energy Technology Laboratory
OH	Ohio
PA	Pennsylvania
ppm	Parts Per Million
REE	Rare Earth Elements
RSD	Relative Standard Deviation

SDD	Silicon Drift Detector
SEM	Scanning Electron Microscopy
τ	Tau
t-SNE	t-distributed Stochastic Neighbor Embedding
TREE	Total Rare Earth Elements
U.S.	United States
USGS	United States Geological Survey
WDXRF	Wavelength Dispersive X-Ray Fluorescence
wt %	Weight Percent
WV	West Virginia
WVGES	West Virginia Geological and Economic Survey
XRD	X-Ray Diffraction
XRF	X-Ray Fluorescence

Regional Investigation of Rare Earth Element-Enriched Underclay Deposits in the Central and Eastern United States: an Earth Mapping Resources Initiative (Earth MRI) Geochemical Reconnaissance Study

Jessica Moore (WVGES), Heather Hanna (Hanna Forensics LLC), Bethany Royce (WVGES), Gary Daft (WVGES), Sarah Brown (WVGES), William Andrews (KGS), and Cortland Eble (KGS)

Abstract

The United States Geological Survey (USGS) Earth Mapping Resources Initiative (Earth MRI) works to identify mineralized areas or deposits across the United States that host critical minerals. Aluminum-rich clays associated with coal horizons represent potentially significant low-grade, large-volume, critical mineral resources. Past studies show that alumina is routinely 20-40% in these clay layers, and preliminary geochemical data indicate that some clay beds host elevated (>300 ppm) rare earth element (REE) concentrations. However, understanding of the distribution of metals in varying lithologies and stratigraphic positions is limited by data density and a lack of modern geochemical data. As part of a first of a kind, multi-year study, over one thousand stratigraphic and spatially representative underclay samples were collected from eight states in the Appalachian and Illinois basins and were geochemically analyzed by the USGS. Initial results of the regional geochemical reconnaissance study showed ranges of total REEs from 1292 ppm to 53 ppm in the Appalachian Basin and 1205 ppm to 8 ppm in the Illinois Basin. Relative enrichment of individual elements was analyzed by tau plots; phosphates and/or Al-rich phases seem to be the primary controls on REE enrichment, while XRD confirmed that the clays' mineralogical content did not hold any REE associated minerals.

Introduction

Aluminum-rich, kaolinitic clays occur in Pennsylvanian strata throughout the Appalachian Plateau Province, the Central Appalachian basin, the Illinois basin, and adjacent areas. These clays are known by various terms (including underclays, fireclays, tonsteins, and Bolivar clays), are generally associated with coal horizons, and have been utilized for brickmaking and pottery for more than 200 years (Eggleston, 1996). The clay-rich units hold potential as an unconventional, low-grade, volumetrically significant critical mineral resource. Regional geology is generally structurally simple, with laterally continuous deposits at or near the surface in areas with long histories of mining and associated infrastructure. The beds are accessible in coal mines, mine face-ups, clay pits, exploration core holes, road cuts, and other outcrops. Given their historical importance as refractory clays, many states hold legacy samples and data in repository collections.

Previous studies of the critical mineral potential of Appalachian coals (Bryan et al., 2015; Rozelle et al., 2016; TetraTech, 2018) suggest low-level Rare Earth Element (REE) enrichment (>300 ppm) in clay-rich mine roof and floor samples (**Figure 1**). Similar clays host high lithium concentrations (>2,000 ppm) (Tourtelot and Brenner-Tourtelot, 1977), and the presence of elevated aluminum makes elevated gallium and indium possible (Conley et al., 1947).

In order to investigate and develop these clays as a possible critical mineral resource, a research team, led by the West Virginia Geological and Economic Survey (WVGES), performed targeted sampling for geochemical analyses in order to investigate the following unknowns: locations and abundances of REEs in high-alumina underclay deposits in the central and eastern U.S.; the mode(s) of enrichment; differential enrichment processes for observed concentrations of Li versus REEs; role of source rocks; regional differences in parent rock type; paleosol weathering patterns; effects of paleogeography on chemical weathering and leaching in Pennsylvanian subtropical to tropical climates; and the role of depositional and

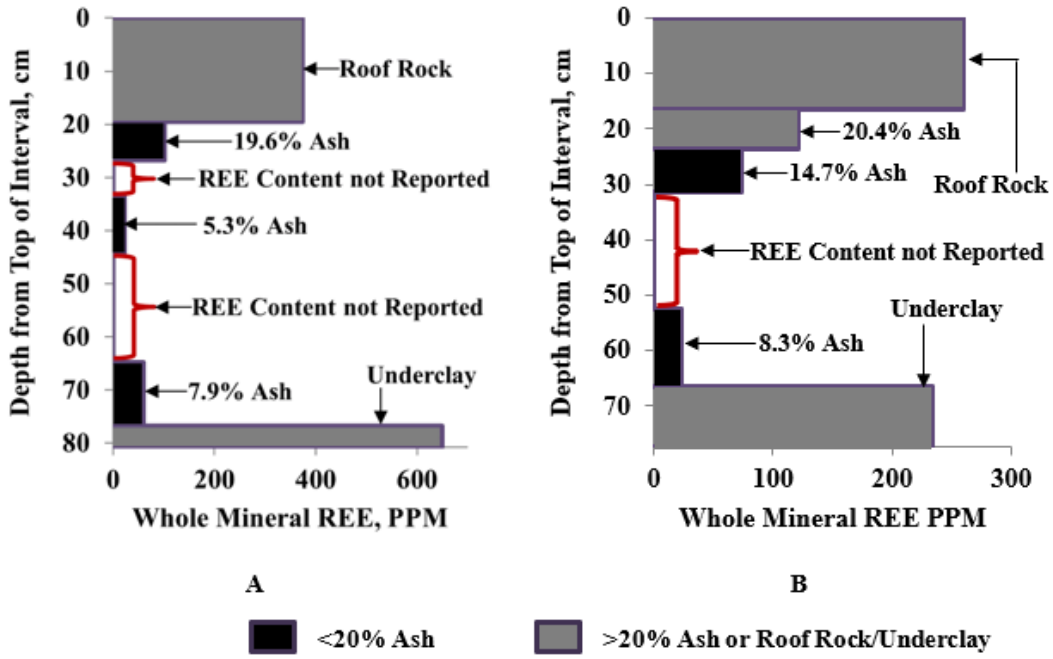

Figure 1*: Modern studies of REEs in the Appalachian Basin suggest enrichment in the clay-rich roof and floor materials in profile of the Lower Kittanning coal in (a) Clarion and (b) Clearfield counties, PA (Rozelle et al., 2016).*

diagenetic factors. Results of this geochemical reconnaissance effort through Earth MRI will help to identify specific stratigraphic intervals of interest and evaluate their regional variations, to determine the presence or absence of elevated concentrations of associated critical mineral commodities, and to inform future studies.

Location and Geologic Background

Pennsylvanian high-alumina clays were deposited during a prolonged period of warm, humid, ever-wet conditions (Cecil et al., 2004) and the resultant intense and pervasive chemical weathering formed well-developed paleosol/ paleolaterite complexes spanning a region extending from western Maryland to Missouri. Key geological units/formations/groups selected for examination include the Pottsville Group and Allegheny Formation (e.g. Mercer, Mt. Savage/Clarion, Ellerslie and Bolivar clay beds of MD, PA, WV, and OH), Olive Hill Clay (Kentucky), and Brazil and Staunton formation underclays (Indiana). Since the study area includes formal and informal stratigraphic bodies correlated between 2 basins focused on age and deposition, unit is used as a broad term. A geological unit consists of rocks of a known origin and age that have distinctively recognizable facies that characterize it, which can include formations and groups in different scales. Although considerable variability exists in these claystone deposits, reflecting varying depositional and subsequent weathering conditions, their history of exploitation, quality, thickness, volume, and widespread distribution provide a potential source for aluminum, REEs, and possibly lithium. Therefore, a regional evaluation of the distribution, chemical character, thickness, and lateral variability of these layers is warranted.

Results of this study will also enable comparison of Paleozoic lateritic deposits to laterites in other Earth MRI projects/focus areas as well as to deposits located in China (Bao and Zhao, 2008; Kynicky et al., 2012; Van Gosen et al., 2017) that constitute a majority of current REE production. When combined, these results can be used to develop a methodology for standardized sampling and analysis of potential

critical mineral-bearing sedimentary clay deposits. These clays have potential for hosting mineral systems and deposit types that commonly contain aluminum, REEs, and future assets such as gallium, hafnium, zirconium and indium (Fortier et al., 2018).

This project is situated in the eastern and central United States and spans a region that extends from the Appalachian basin through the Illinois basin and into eastern and central Iowa. While residual claystone intervals are known throughout the Pennsylvanian strata of the Appalachian and Illinois basins, those found within Lower and Middle Pennsylvanian units are of different character than those of the later Carboniferous (Brezinski and Kollar, 2011) **(Figure 2)**. This succession of stratiform claystone units were formed by intense ancient weathering processes during a period of Earth's history stretching from 318 to 307 Mya.

Keller et al. (1953) recognized the significance of one of these thick lower Pennsylvanian clay intervals, the Cheltenham Clay of eastern Missouri. This widespread unit occupies the stratigraphic interval between the Morrowan and lower Desmoinesian (equivalent to the Pottsville Group through Allegheny Formation in the Appalachian basin) and is distributed throughout southeastern and central Missouri. Cecil et al. (2004) proposed that the Cheltenham of Missouri was correlative to the Olive Hill Clay of Kentucky (Patterson and Hosterman, 1958) and the Mercer Clay of central Pennsylvania (Williams, 1960). The Mercer is distributed across a substantial part of the Appalachian Plateaus Province of central Pennsylvania, is up to 3 meters thick (Williams and Bragonier, 1974; 1985), and was formed on the latest Mississippian-early Pennsylvanian surface exposed during the widespread mid-Carboniferous unconformity (Beuthin, 1997; Rygel and Beuthin, 2002; Blake and Beuthin, 2008). Thus, these contemporaneous units represent prolonged periods of early Pennsylvanian subaerial exposure and deep leaching that affected a significant area in the eastern and central United States (Keller et al., 1954; Williams and Bragonier, 1974).

Given the wide geographic expanse and diverse framework geology, input from individual state surveys was necessary to form a comprehensive study of the critical mineral potential of clays in the region. A total of eight state geological surveys contributed to the effort, and the resultant work is divided into two groups: an Appalachian basin group comprising the states of Maryland, Pennsylvania, West Virginia, Ohio, and eastern Kentucky; and a western group spanning the Illinois basin into Iowa and including western Kentucky, Indiana, Illinois, and Iowa **(Figure 3)**.

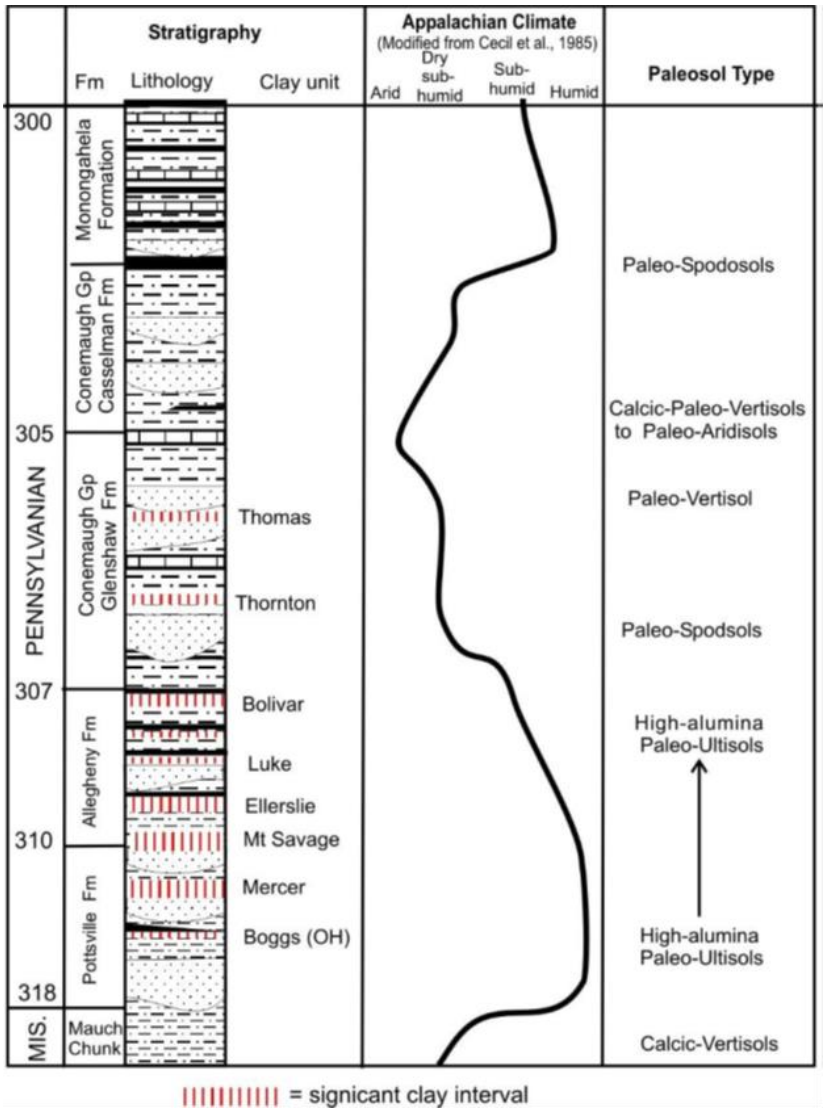

Figure 2. *Pennsylvanian stratigraphy, including major high-alumina clays identified in Maryland. Pennsylvania, and West Virginia (Brezinski and Kollar, 2011).*

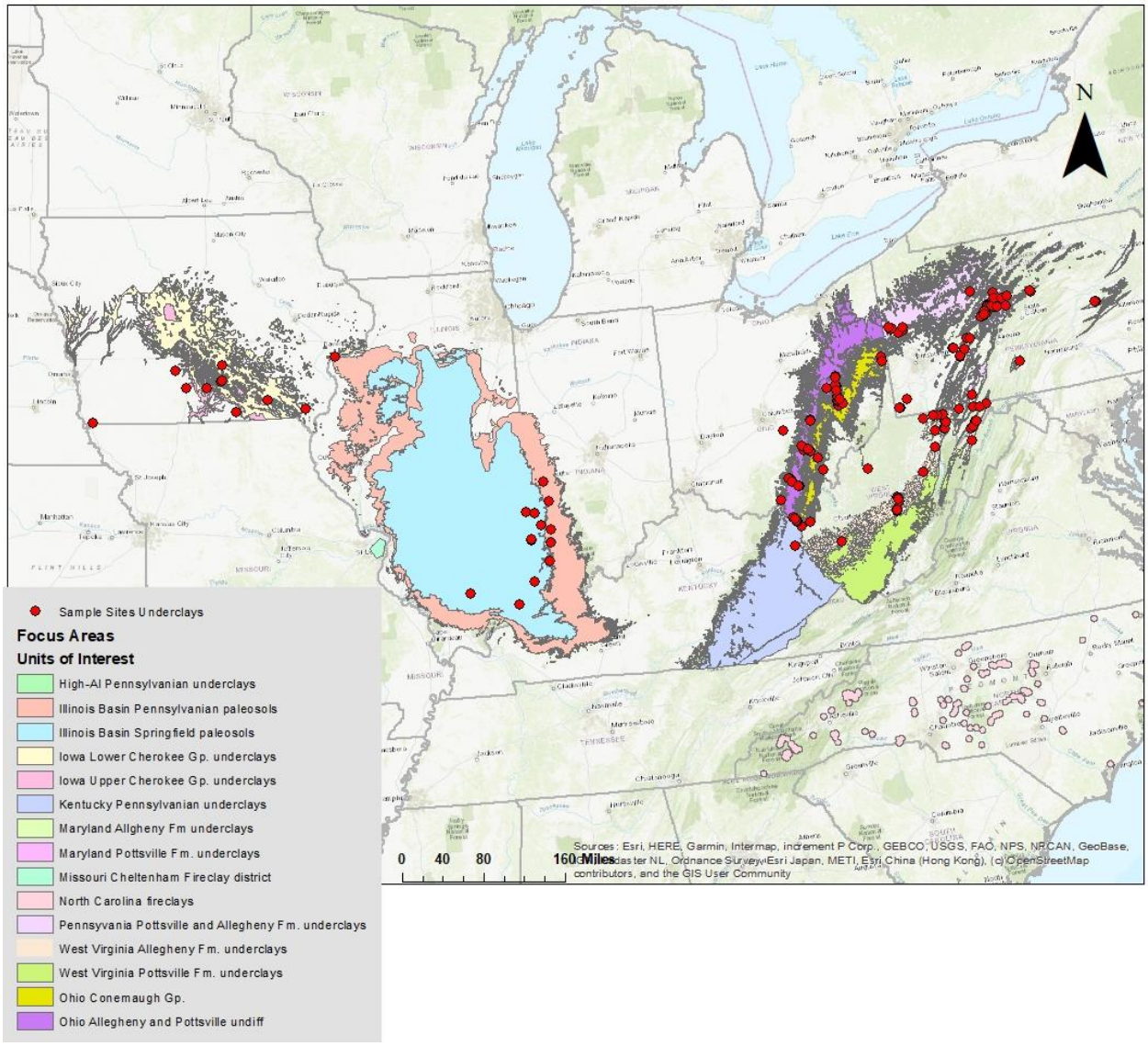

Figure 3. *Map of study area with local stratigraphic units and sample locations.*

Methodology

Sampling

Sampling work in support of this project follows the Mineral Systems Approach guidelines developed by USGS EMRI (Hofstra and Kreiner, 2020) to evaluate potential critical mineral deposits. A two-phased approach was used to collect a stratigraphically and spatially representative sample suite for this study that consisted of a total of 1,061 samples. Phase 1 goals were to determine and locate stratigraphic and lithological intervals with the greatest promise of hosting elevated critical mineral resources. Travel restrictions due to COVID-19 prevented field work and travel across the states to explore and collect new samples from outcrop, so Phase 1 sampling plans were modified to collect from drill core held by the surveys and augmented by samples taken from local outcrops and quarries. In Phase 1, 199 samples were submitted to the USGS from the Illinois basin and 312 from the Appalachian basin, for a total of 511 samples. Methodology for core sampling with an example from WV can be found in **Appendix I** along with detailed stratigraphic logs from the

cores chosen for this study. Phase 2 samples were collected in the field once travel restrictions were lifted. Sample locations for Phase 2 were informed by Phase 1 results and also targeted locations of interest from the literature or from previously measured outcrop sections. During Phase 2, 90 samples were sent to the USGS from the Illinois Basin and 460 samples from the Appalachian Basin, for a total of 550 samples.

ICP-OES-MS and WDXRF

Geochemical analyses of all samples were performed by AGAT Laboratories under contract from USGS. The methods used include a whole-rock Wavelength Dispersive X-Ray Fluorescence (WDXRF) package and a total digestion Inductively Coupled Plasma-Optical Emission Spectroscopy-Mass Spectroscopy (ICP-OES/ICP-MS) 60 element package. These methods were used to ensure consistency and comparability across all Earth MRI geochemical analyses, to meet USGS requirements for quality, and to be compatible with existing geochemical datasets. The combined WDXRF and 60 element packages were provided along with requisite sample processing, appropriate quality control samples, duplicates, and data validation. To monitor the quality of data generated by the contract laboratory, quality control and duplicate check samples were submitted with each set of samples. These samples were analyzed by the same analytical methods described previously.

Major elements were determined in the samples by WDXRF; the samples were fused with lithium metaborate/lithium tetraborate flux and the resultant glass disk was introduced into the WDXRF and irradiated by an x-ray tube. The method also provides a gravimetric Loss on Ignition (LOI). The data were considered acceptable if recovery of each major oxide was ±5% at five times the lower Limit of Determination (LOD) and the calculated Relative Standard Deviation (RSD) of duplicate samples was no greater than 5%. Through ICP-OES-MS sixty elements were determined in the samples. They were fused at 750°C with sodium peroxide, the fusion cake dissolved in a dilute nitric acid, and the resulting solution was then analyzed by ICP-OES and ICP-MS. The data were deemed acceptable if recovery of each element is ±15% at five times the LOD and the calculated RSD of duplicate samples is no greater than 15%.

Handheld X-Ray Fluorescence (hhXRF)

In order to test the hypotheses from statistical modeling from Orange, an open-source machine learning and data visualization software, (methodology for Orange is provided in **Appendix II**), 461 samples were analyzed with a Bruker Tracer i5 Handheld X-Ray Fluorescence (hhXRF) spectrometer equipped with a SDD graphene window detector and 50 kV Rh X-ray tube. Analyses were either conducted on the sample surface or samples were powdered using a mortar and pestle and tested in a sample mount. All samples were run with air under an 8mm spot window. Two different applications were run to test the variability of the applications. MudrockAir Dual, a calibration for sedimentary rocks with the elemental range of Na-U, was conducted at 90/180 second phase intervals and GeoExploration, calibrated for oxide analysis of certain elements with the elemental range of MgO to U was conducted at 60/60/60 second intervals. All data was reported in weight percent (wt %) and then converted to parts per million (ppm). If data were reported with <LOD or if the error is more than the reported value, the element is not detected.

X-Ray Diffraction (XRD)

A total of 27 samples were selected by project researchers for mineralogical characterization by X-ray Diffraction (XRD). Splits were received from USGS Geology, Geochemistry, and Geophysics Sample Control after having been crushed and homogenized, following the preparation method described in User's Guide to Rockjock (Eberl, 2003). Each sample was passed through a 200-mesh sieve (<74 microns), then 1.0 g of sample was mixed with 0.250 g of corundum, and ground with about 5 ml of methanol in a McCrone micronizing mill for 5 minutes using zirconia grinding elements. The mixture then was dried overnight at about 30° C. The sample plus corundum mixture then was shaken in a plastic scintillation vial (20-25 ml) with 3 plastic balls (10 mm diameter) to mix the sample and corundum well. Next Vertrel™ was added to the mixture in the ratio of 0.5 mL Vertrel™ to 1 g of sample, and the vial shaken again for 10 minutes.

The powder is then passed through the sieve again, and side loaded into an XRD holder.

The samples were scanned using PANalytical "X'Pert Pro – MPD X-ray Diffractometer with Theta/Theta geometry, Cu long-fine-focus X-ray tube (Ni filtered), and an "X'celerator" solid state "strip" detector. X-ray tube conditions were 45 kV, 40 mA with a 15 mm beam mask, ½° anti-scatter slit, ¼° divergence slit, ½° receiving anti-scatter slit, ¼° receiving divergence slit, and the step size was 0.0167° in continuous scan mode with a scan range of 4° to 70° two-theta. With the sample spinner on, the total scan time is 1 hour 18 minutes.

Identification of mineral phases utilized Material Data Inc. Jade (Pro version) search-match software using the ICDD's "2021 PDF-4" and National Institute Standards and Technology "FIZ/NIST Inorganic ICSD" databases installed. Semi-quantitative mineral estimates were calculated using MDI Whole Pattern Fit software that simultaneously calculates a whole pattern fit and a Rietveld refinement of the minerals. Reference minerals were then selected from the database, some of which are "structure" references that represent perfect crystals of the mineral and other entries are real world mineral specimens. Each of these cards contains a full crystallographic description of the mineral. A calculated model of the observed pattern is produced by non-linear, least-squares optimization and the calculations, performed by the software, involve the application of various parameters to improve the fit of the model to the observed data. Modeling parameters include background reduction, profile fitting, and lattice constraints that iterate minimizing a residual error between the calculated x-ray diffraction pattern from selected references in comparison to the measured scan of the sample. Mineral contents are normalized to 100% based on the identified minerals. A full description of the Whole Pattern Fit algorithm is available through MDI software.

Tau (τ) Calculation and Parent Composition Selection

Volumetric changes accompany chemical weathering, which can complicate interpretations of concentration data. To overcome these complications, the mass balanced-based $\tau_{j,w}$ values have been adopted (Brimhall and Dietrich, 1987; Chadwick et al., 1990; Anderson et al., 2002). $\tau_{j,w}$ represents the percent mass change of a mobile element j, in a weathered sample relative to the mass of the same element in the parent rock (Anderson et al., 2002). It is calculated as

$$\tau_{j,w} = \frac{C_{j,w}C_{i,p}}{C_{j,p}C_{i,w}} - 1$$

where C represents the concentration of a mobile element, *j*, or an immobile element, *i*, in a weathered sample, *w*, or the parent composition, *p*. Niobium (Nb) is used as the immobile element in this study due to its documented immobility during weathering (e.g., Hill et al., 2000; Kurtz et al., 2000; Ma et al., 2011). Negative τ values indicate a net loss of the mobile element has occurred, positive values indicate a net gain, and a value of zero indicates no net change. A τ value of -1 means the mobile element is 100% depleted relative to the parent composition, while a τ value of 1 indicates the element is 100% enriched relative to the parent composition. Tau values cannot be less than -1 since a net loss greater than 100% is not possible, however positive (enrichment) values can go as high as geologic processes allow.

Since underclay parent compositions are unknown, the practice of selecting the least weathered sample was used in this study. To identify the least weathered sample, Chemical Index of Alteration (CIA) and Index of Laterization (IOL) values were calculated for all ~227 samples for which data were available at that time. CIA is a weathering index that primarily reflects feldspar dissolution and the resulting loss of mobile CaO, Na_2O, and K_2O relative to Al_2O_3, the latter of which is presumed to be immobile due to its incorporation into pedogenetic clay minerals (Babechuk et al., 2014). CIA is calculated as the molar ratios of $[Al_2O_3/(Al_2O_3+CaO^*+Na_2O+K_2O)]x100$, with CaO* representing the CaO in silicate phases after the contribution from carbonates and apatite has been removed (Nesbitt and Young, 1982). As the mobile elements become more depleted, CIA values become less reliable, so IOL values were also calculated. IOL is a weathering index that

reflects SiO_2 loss during kaolinization and other highly advanced stages of chemical weathering relative to more immobile Al_2O_3 and Fe_2O_3. IOL is calculated as the molar ratios of $[(Al_2O_3+Fe_2O_{3(T)})/(SiO_2+ Al_2O_3+ Fe_2O_{3(T)})]x100$, with $Fe_2O_{3(T)}$ representing total iron concentration as Fe_2O_3 (Babechuk et al., 2014 and references therein).

To better understand the impact of parent composition on tau plots for Appalachian basin underclays, the five samples with the lowest CIA and IOL values were identified, and a series of tau plots were constructed using each sample as the parent composition. Additional tau plots were constructed for comparison purposes using the Cody Shale and North American Shale Composite as parent compositions. Overall tau patterns were identical for all "parent compositions" with the notable difference being how far each element's pattern was shifted towards enrichment or depletion. To account for this variation, percentages of enrichment or depletion indicated by study tau plots should be regarded as estimates instead of absolute values. The average of Kentucky Geological Survey (KGS) samples KGSc334-87.3 and KGSc334-87.3Q was selected as the final parent composition and denoted as KGSc334-87.3ave. An average was calculated for the samples because they are from the same depth in the same core and have elemental concentrations within analytical error of each other. KGSc334-87.3ave has a CIA value of 35.6, which is the lowest of the calculated CIA values. For reference, fresh igneous rocks have CIA values ranging from 35 to 53, with felsic compositions falling toward higher values and mafic to ultramafic rocks falling toward lower values. Idealized montmorillonites and illite have CIA values between 75 and 85, and idealized kaolinite plots close to 100 (Nesbitt and Young, 1982). Additionally, Eu/Eu* values for the KGSc334-87.3ave were compared to samples from the rest of the unit to ensure local feldspar accumulation had not impacted the CIA value by artificially inflating mobile element concentrations at that depth. Sample KGSc334-87.3ave also had the lowest IOL value (16.7) which is well below the lower limit for kaolinization (IOL = 57; Babechuk et al., 2014). Finally, since Nb is the immobile element used in all calculations, the Nb concentration for KGSc334-87.3ave was compared to that of the other low CIA samples to confirm the value did not seem suspiciously high or low.

Results and Discussion

ICM-OES-MS and WDXRF

Analytical results were received periodically from USGS/AGAT labs throughout the period of investigation and were compiled separately for the Illinois and Appalachian basins. From each state, the top five samples with the highest total REE (TREE) concentrations were reported from the 1,061 samples analyzed for this report. TREE calculations include the following elements: Ce, Dy, Er, Eu, Gd, Ho, La, Lu, Nd, Pr, Sm, Tb, Tm, and Yb; these are shown in **Table 1** along with TREE+Y and TREE+Y+Sc for the top five samples in each state, as Sc and Y elements are often included as TREE in the literature.

At the outset of the geochemical reconnaissance study, other critical or industrial minerals were identified from the literature as potentially associated with REE-bearing clays. These include aluminum, gallium, indium, and lithium.

Concentrations of aluminum (Al) analyzed by ICP-OES-MS ranged from 20.7% to 0.25%. Concentrations of Al_2O_3 analyzed by WDXRF ranged from 41.09% to 0.48%. More than half of the samples had concentrations of Al_2O_3 greater than 20% but only one sample in Clearfield County, Pennsylvania measured greater than 40%. Although some of the top five samples per state have high values of Al_2O_3, 12 out of the 40 top TREE concentrations measure less than 20%.

All samples had gallium (Ga) present with values ranging from 62.3 ppm to 8.12 ppm; 936 of the 1,061 samples had Ga values above the average crustal abundance of 19 ppm (Foley et al., 2017), including all but two of the top five samples from each state. Concentrations were generally higher in the Appalachian basin.

In contrast, only 20 samples across both basins had indium (In) present; values range from 1 ppm

to 0.2 ppm. The highest indium concentration (1ppm) was found in Daviess County, Indiana; a majority of the other concentrated samples were located in the Appalachian basin. Only one of the top five TREE samples had indium present.

Lithium (Li) is present in 1,040 of the 1,061 samples; concentrations range from 1,100 to 11 ppm. The highest concentration, 1,100 ppm, was observed in the Appalachian basin in Lawrence County, Pennsylvania. The highest lithium concentration in the Illinois basin was 662 ppm from Appanoose County, Iowa.

Chondrite-normalized REE values were given for each sample based on bulk rock composition. An element's chondrite normalized composition is the ratio of its concentration in the sample to the average CI carbonaceous chondrite. Plots using Boynton (1984) for normalization were created for each of the eight states to show variability within their samples **(Figures 4 & 5)**. Chondrite curves from Iowa and Maryland follow the same trend with little internal variability. Curves from Illinois, Pennsylvania, and West Virginia have a strong trend with some noticeable outliers, and Indiana and Kentucky plots show the greatest variability within the samples. The charts also show that most states have an enrichment of light REEs compared to heavy REEs. See **Appendix III** for ICP-OES-MS and WDXRF data.

Illinois

Out of the 43 samples collected from Illinois, 6 samples had TREEs higher than 300 ppm (~14%), ranging from 475.01 to 330.27 ppm. All the top five samples are drill core samples from Franklin County, collected from mudstones within the Carbondale Formation. Two of the highest TREE concentrations, (475.01 and 330.27 ppm), were collected from mudstones near the Colchester coal. Samples from the Davis coal horizon comprised an additional two of the top five values (427.29 and 401.47 ppm), and a final top value of 408.23 ppm was observed in a sample from the Danville Coal #7.

Indiana

Of the 154 samples collected from Indiana, 14 had TREEs higher than 300 ppm (~9%), values range from 1,205 ppm to 493.75 ppm. A sample from Sullivan County had the second-highest TREE measured in the study (1,205 ppm). All top five samples were collected from drill cores. The highest TREE concentrations, 1,205.93 in Sullivan County and 690.05 ppm in Knox County, were observed in paleosols associated with the Danville coal in the Dugger Formation. In Clay County a sample from a paleosol beneath the Wise Ridge Coal in the Staunton Formation measured 580.5 ppm, a similar paleosol sample collected beneath the Upper Block Coal in the Brazil Formation in Daviess County measured 533.04 ppm, and a sample from Pike County in the Carrier Mills Shale in the Staunton Formation measured 493.75 ppm.

Iowa

Fewer than 10% of samples collected from Iowa had TREEs higher than 300 ppm (6 of 70 samples); elevated values ranged from 456.76 to 315.92 ppm. The highest TREE concentration (456.79 ppm) was observed in a mudstone within the Floris Formation, approximately 3 feet below the lower North Coal in Davis County. The remaining four highest TREE concentrations were from drill core samples in Clarke County. Two samples from the Lower Pennsylvanian Bandera Shale Formation measured 450.11 and 361.25 ppm, respectively. A mudstone sample collected from the Pleasanton Group measured 431.74 ppm, and a mudstone from the Memorial Shale Formation measured 315.92 ppm.

Kentucky

Twenty-five percent of samples collected from Kentucky had TREE concentrations greater than 300 ppm (24 of 96); values ranged from 812.25 to 486.35 ppm. All samples from Kentucky were taken from drill core in Union County and all are claystone, with the exception of one shale. The highest enrichment (812.25 ppm) was observed in a sample collected from the Hitchens clay bed in the Princess Formation. The remainder of the most enriched samples were taken from the Tradewater Formation; three of those samples were from the WK6 zone paleosol. The WK6 zone paleosols had TREE measurements of 810.4, 787.65 and 615.66 ppm, respectively. The fourth Tradewater Formation

sample was collected from a separate paleosol and measured 486.35 ppm.

	TREE	TREE+Y	TREE+Y+Sc		TREE	TREE+Y	TREE+Y+Sc
Illinois				**Indiana**			
2466700_1024.2	475.01	517.21	532.21	SDH-4-6	1,205.93	1,280.13	1,302.13
2466700_1080.6	427.29	526.29	548.29	SDH-259-6	690.05	728.55	748.55
2466700_691.8	408.23	503.03	520.03	SDH-317-7	580.5	606.5	639.5
2466700_1081	401.47	452.97	472.97	14Q13-17	533.04	635.04	661.04
2466700_1021.5	330.27	369.67	386.67	SDH-379-13	493.75	701.75	719.75
Iowa				**Kentucky**			
SC20-3	456.79	517.21	532.21	KGSc334-268.8	812.25	860.65	911.65
CP37-14	450.11	526.29	548.29	KGS546-631.5	810.46	866.93	882.93
CP37-24	431.74	503.03	520.03	KGS546-619.5	787.65	837.15	861.15
CP37-8	361.25	452.97	472.97	KGS546-625.5	615.66	675.46	694.46
CP37-20	315.92	369.67	386.67	KGS546-779	486.35	515.95	534.95
Maryland				**Ohio**			
MD-4-I	763.66	791.06	826.06	OSG-CSH0062C	1,292.86	1,320.86	1,332.86
MD-12-L	470.1	503.8	521.8	OSG-CSH0062B	580.56	620.56	642.56
MD-13-A	458.03	512.93	536.93	OSG-CSH0066B	558.98	597.48	631.48
MD-3-A	420.3	467.6	490.6	OSG-CSH0026	512.73	551.03	575.03
MD-7-B	411.33	450.43	478.43	OSG-CSH0042D	499.36	550.36	575.36
Pennsylvania				**West Virginia**			
IND063_2361_99.0FT	668.01	750.41	772.41	WV-EMRI-204	923.54	998.84	1031.84
IND063_2363_54.46FT	620.75	677.55	717.55	WV-EMRI-203	631.79	690.89	723.89
MRI-22-C	602.31	629.41	642.41	50-092A-B1	595.59	638.19	649.19
MRI-4-B	571.76	618.36	642.36	WV-EMRI-087	593.2	613.4	638.4
MRI-28M	541.73	586.93	619.93	WV-EMRI-014	581.32	615.42	655.42

Table 1. Values of Total REE, TREE+Y, and TREE+Y+Sc of the top 5 samples in each state.

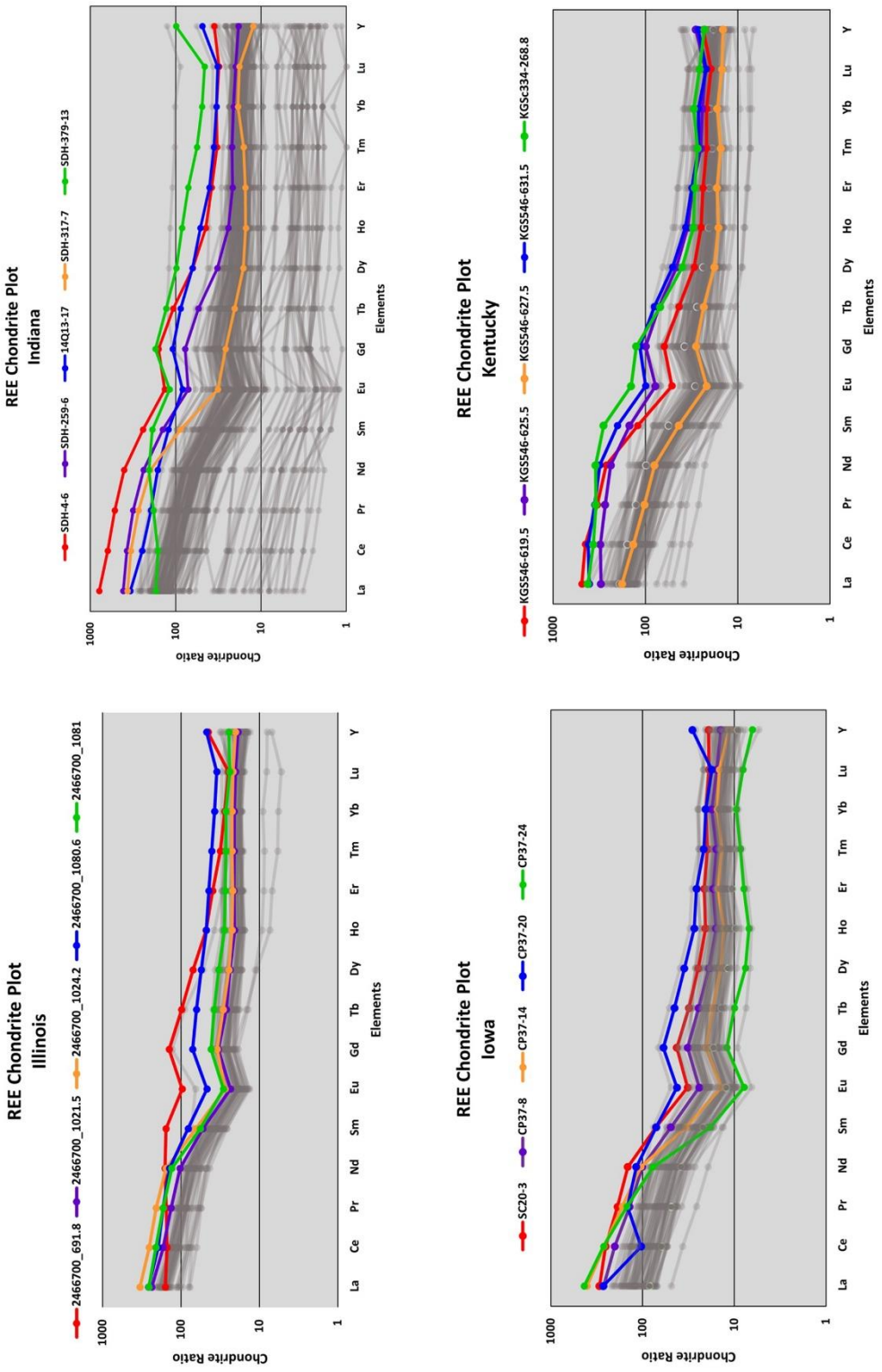

Figure 4. *Normalized chondrite ratios for each state highlighting the top 5 highest REE samples.*

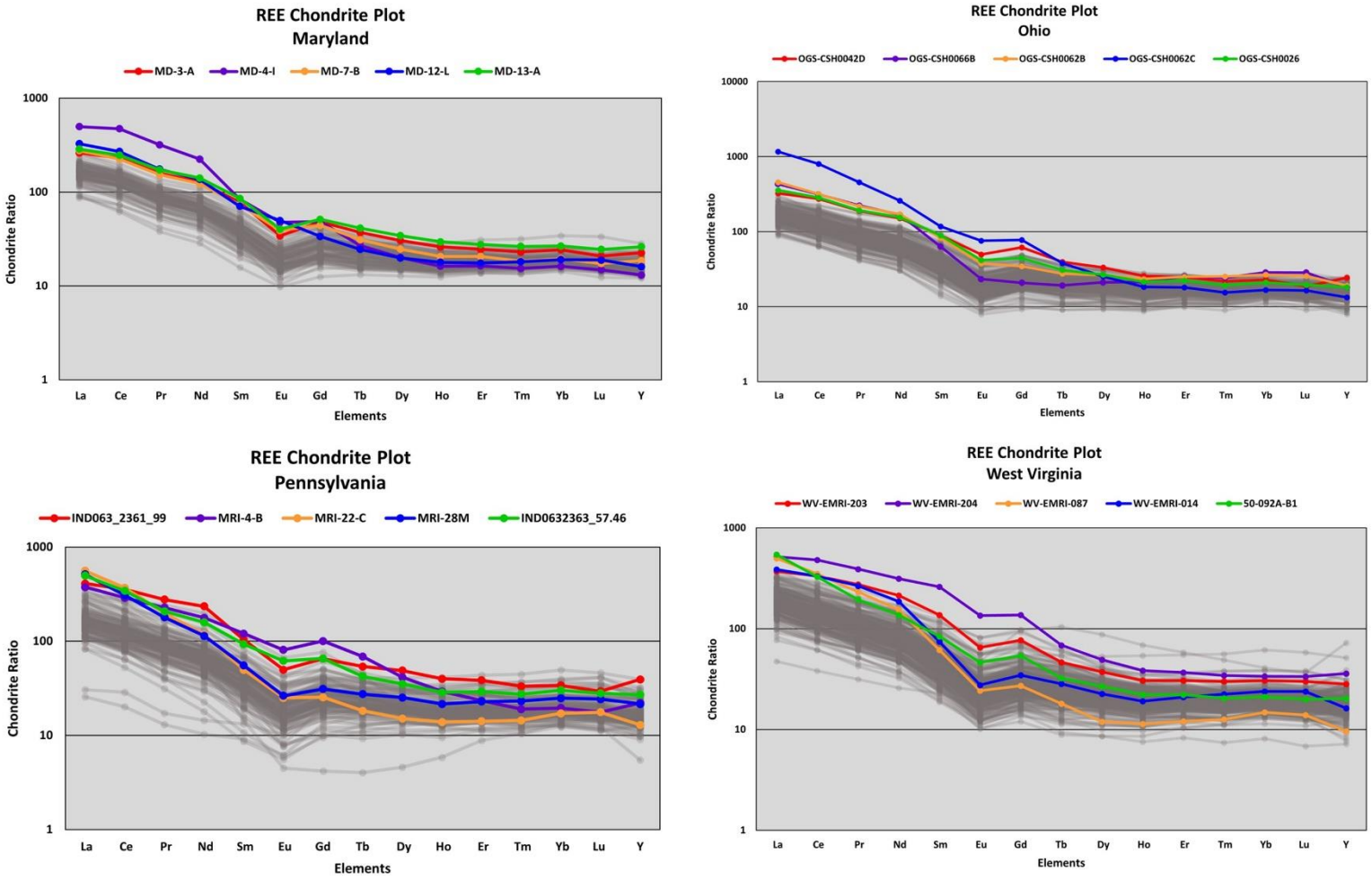

Figure 5. *Normalized chondrite ratios for each state highlighting the top 5 highest REE samples continued.*

Maryland

Of the 100 samples collected from Maryland, 14 (14%) had TREEs higher than 300 ppm. All the top 5 highest TREE concentrations were collected from claystones in outcrop, but it should be noted that sample MD-4-I was collected from a location in Grant County, West Virginia. This sample, collected from an exposure that includes the Mercer (Upper Pottsville Fm.) and Mt. Savage (Lower Allegheny Fm.) claystones, measured 763.66 ppm TREE. The remaining top samples from Maryland were all collected from Garrett County and include a sample of the Mt. Savage claystone collected below the Clarion coal in the Allegheny Formation on Big Savage Mountain (470.1 ppm), a second sample from the same locality collected below the Middle Kittanning coal in the Allegheny Formation (458.03 ppm), a sample of the Bolivar claystone below the Upper Freeport coal in the Upper Allegheny Fm. from a locality west of Luke, MD (420.3 ppm), and a Bolivar claystone sample collected from Big Savage Mountain (411.33 ppm).

Ohio

Seventeen percent of samples collected from Ohio had TREE content higher than 300 ppm (35 of 206 samples), and a sample from the Clarion underclay (Allegheny Fm) in Lawrence County measured the highest TREE observed in the study (1,292.86 ppm). Two additional Clarion underclay samples in Lawrence County measured 580.56 ppm and 558.98 ppm. A fourth sample from the Allegheny Formation in Guernsey County collected beneath the Upper Freeport coal measured 512.73 ppm, and a sample from the Huckleberry underclay (Pottsville Fm.) in Jackson County measured 499.36 ppm.

Pennsylvania

Eighteen percent of samples collected from Pennsylvania had TREE content greater than 300 ppm (23 of 128 samples); the five samples with highest enrichment were all collected from claystones and values range from 668.01 to 581.32 ppm. Highest enrichment (668.01 ppm) is observed in a sample taken above the Mauch Chunk-Pottsville formational contact in Indiana County. Three of the top five samples were collected from the Mercer complex within the Pottsville Formation. A sample taken directly below the base of 0.28-feet thick coal-shale-coal package in the Mercer complex in Lawrence County measured 620.75 ppm, a sample from the Mercer underclay, a flint clay on the Mississippian - Pennsylvanian boundary, in Clearfield County measured 602.31 ppm, and a sample from a local coal located 10 ft. below the Lower Mercer coal and 1.7 ft. above the “Flint Ridge” coal also from Clearfield County measured 541.73 ppm. Only one sample from the Allegheny Formation was included in the top five samples in Pennsylvania. This sample was collected from the Lower Kittanning underclay in Lawrence County and measured 571.76 ppm.

West Virginia

West Virginia had the highest proportion of enriched samples, with TREE enrichment over 300 ppm observed in 86 of 266 samples (32%); values range from 923.54 to 581.32 ppm. All of the top five samples are claystones from the Allegheny Formation; four were taken from drill cores and one from outcrop. The two highest TREE concentrations (923.54 and 631.79 ppm) were derived from samples collected ~10 feet below the base of the Middle Kittanning coal in Ritchie County. Two of the top samples were collected from Braxton County, including an outcrop sample (TREE = 595.59 ppm) and a sample taken from ~35 feet below the Brush Creek coal horizon between the Glenshaw and Allegheny Formations (TREE = 593.2 ppm). A final sample from the base of the Clarion coal zone in Monongalia County measured 581.32 ppm.

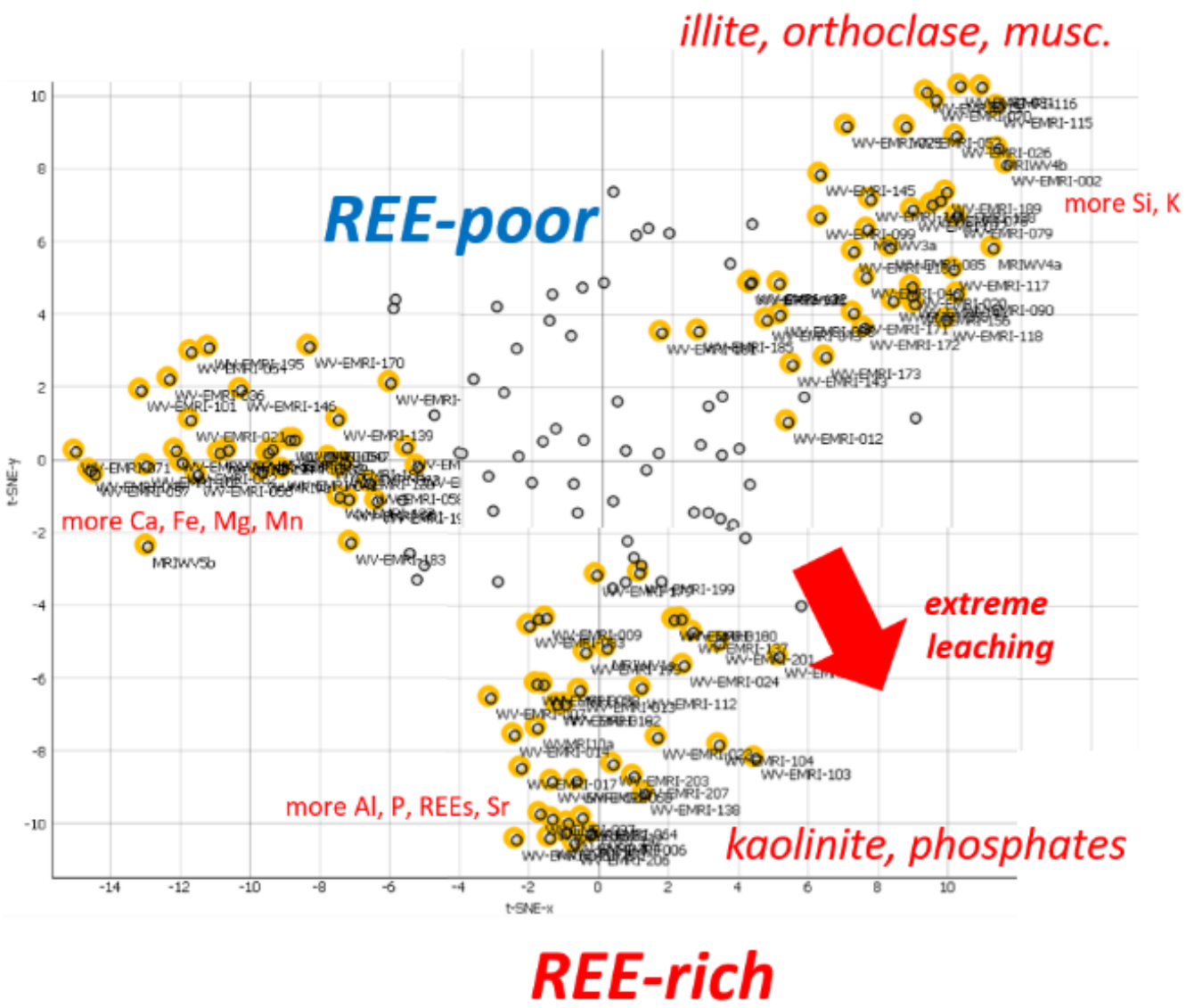

Figure 6. t-SNE plot showing grouped elements based on their probability distribution related to minerals and REEs.

hhXRF and Orange

After running Orange through several iterations, trends that indicate higher REE totals (> 375 ppm) were identified, including an inverse correlation with total REEs with Mg < 3800 ppm and strong positive correlations with total REEs with:

- Al > 137,500 ppm;
- Ba > 670 ppm;
- Cr > 130 ppm;
- Cu > 56 ppm;
- 26,500 ppm > K > 18,750 ppm;
- P > 500 ppm;
- Pb > 39.5 ppm;
- Sr > 500 ppm; and
- Th > 20 ppm

and weakly positive correlations with total REEs with:

- Bi > 0.7 ppm;
- Ga > 37.5 ppm;
- Nb > 20 ppm;
- Sb > 1.3 ppm;
- Ti > 7,000 ppm;
- U > 6.5 ppm; and
- V > 170 ppm.

Multidimensional space (MDS) along with t-distributed Stochastic Neighbor Embedding (t-SNE) plots show correlations and general similar behavior of REES with Cu, Cr, Pb, U, Sb, V, Bi, Ga, and Ba. (**Figure 6)** Plots indicate that the REEs are mainly in kaolinite; a relative lack of Al and K suggests that illite is not the dominant clay mineral. REEs appear to occur in a mix of kaolinite, chlorite, and smectite.

Predominance of kaolinite indicates heavy weathering and saprolite production, with less input of erosional detrital allogenic minerals as source of REEs. The cyclical occurrence of clays within and under coals (cyclothems tied with Gondwana glaciation) suggests weather-related deposition of clays and coals rather than tectonic controls (uplift and erosion in eastern Laurentia). REE-bearing minerals do not seem prevalent; there is not remarkably high P or Th concentrations together with REE, indicating significant amounts of monazite and/or xenotime are absent. Few samples exhibit high Zr and Hf concentrations, which indicates there is not abundant zircon. There are some hints of Sr with P in a few samples which may indicate Sr-phosphates such as florencite, goyazite, and belovite.

The abnormal association of total REEs with transition metals such as Pb, Cu, Sb, Cr, V, and Bi is atypical of common REE minerals like monazite, xenotime, or bastnasite and allows for the predominance of ion absorption clays to be the main host. The Al content is extremely high due to a very high degree of weathering, as other elements are stripped out, immobile Al remains and indicates longer and greater amounts of weathering. This places the REEs and additional critical minerals mentioned here in the Appalachian basin within the Chemical Weathering System of the USGS defined mineral system approach (Hofstra and Kreiner, 2020). See **Appendix II** for Orange related data.

Although the Orange predictions hold true for some samples, it is not accurate at predicting all or the majority high REE samples. Future work will involve adding the rest of the Earth MRI results into the Orange software to see if it can further constrain the predictions, as well as testing the sample splits received from the USGS with hhXRF.

With the ICP-OES-MS data providing TREE data, comparisons to the hhXRF results were evaluated without Orange to ascertain any possible correlations between known high REE samples and the hhXRF elemental data. Based on observations of values within the hhXRF data in the MudrockAir Dual calibration, 6 elements produced high REEs:

- Ba > 1200ppm;
- Ga > 63 ppm;
- Nb > 50 ppm;
- Sr > 350ppm;
- Th > 50ppm; and
- Y > 55 ppm.

The observations of values within the hhXRF data in the GeoExploration calibration found 7 elements that correlated with high REEs:

- Ba > 1000ppm;
- Ga > 40ppm;
- P > 3000ppm;
- Sr > 500ppm;
- Th > 70ppm;
- U > 50ppm; and
- V > 600ppm.

Some commonalities emerge between the machine learning (ML) results and direct observation of hhXRF measurements from both instrument calibration packages. Associations between total REES and barium, strontium, and thorium are observed in the ML results and hhXRF calibrations. All of the elements identified in the ML associations as being strongly or weakly positively correlated with total REE were also identified in the hhXRF calibrations. These preliminary observations warrant more data and research to help guide future strategies for in-field sample screening. See **Appendix IV** for hhXRF data.

X-Ray Diffraction (XRD)

27 samples were selected to have XRD analyses performed, including Rietveld and clay specification, to determine the mineral forms/species. XRD selection was informed from Phase 1 sampling results, hhXRF, legacy data, and machine learning analyses. These samples were selected in order to confirm that the clay is dominantly kaolinite, as indicated by the machine learning results and CIA bulk geochemical values, and to determine if REE-specific minerals are present in the clay. Initial whole rock data indicates that the majority of the clays are kaolinite, but both kaolinite and illite are present in varying amounts in all samples except for MD-6-D. REE-specific minerals are not observed in the XRD results, confirming that the REEs are not contained within monazite, xenotime, bastnaesite or other minerals but rather are free throughout clays.

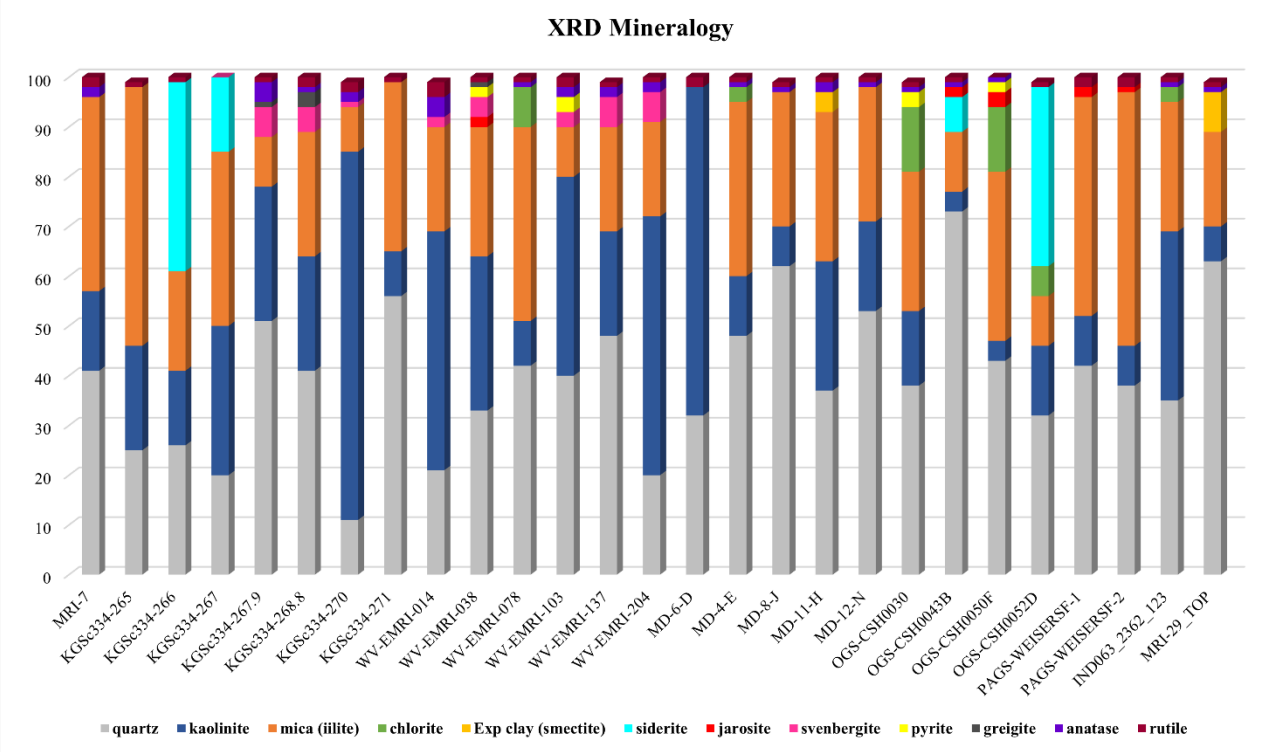

Figure 7. *XRD mineralogy results*

From the samples sent to the USGS, twelve minerals were identified: kaolinite, mica (illite), chlorite, expanding clay (smectite), quartz, siderite, jarosite, svanbergite, pyrite, greigite, anatase, and rutile. All 28 samples reported kaolinite and quartz. Illite and rutile were reported in 26 of the 27 samples, and anatase was reported in 18 of the samples. Less common minerals included svanbergite (8 of 28 samples), chlorite (6 samples), jarosite (5 samples), siderite and pyrite (4 samples, respectively), greigite (3 samples). Smectite was only reported in 2 of the samples. (**Figure 7**) See **Appendix V** for XRD data.

Notable among the minerals identified by the XRD analysis are svanbergite, an uncommonly observed compound sulfate-phosphate of Sr and Al, and jarosite, a member of the alunite group that forms as a secondary mineral on Fe-rich rocks. With known limitations of XRD, follow up work will include using scanning electron microscopy (SEM) to verify that REEs are free throughout the clays and not contained within minerals.

Tau Plots

REEs have similar chemical properties which cause them to behave in an overall similar manner in the environment (Tyler, 2004; Laveuf and Cornu, 2009). However, differences in size and atomic structure cause subtle behavioral differences between the Light REE (LREE; La to Nd), Middle REE (MREE; Sm to Dy) and the Heavy REE (HREE; Ho to Lu) during weathering. In particular, HREE are more mobile because they form more stable complexes with colloids while LREE are more soluble, meaning they are more likely to be present as free species (Cantrell and Byrne, 1987; Kurtz et al., 2001; Laveuf and Cornu, 2009). MREE span the difference between HREE and LREE, with heavier MREE behaving more similarly to HREE and lighter MREE behaving more similarly to LREE. These differences in REE behavior impact the likelihood of retention in a profile and can provide insight into the processes that impacted REE concentration and distribution.

Chemical weathering releases REE into solution, where they can migrate into, out of, and throughout a weathering profile based on their relative mobility and solubility. While chemical weathering is releasing REE into the environment, it is also breaking down existing minerals causing new minerals to form. This process enables retention of REE in two primary ways. First, REE can substitute for other elements in these new minerals, which can lead to their retention in the profile. Second, REE can adsorb, or stick to the surface of minerals, amorphous phases, and organic material. Adsorption is the more important of the two mechanisms for both clay minerals (Coppin et al., 2002) and Fe oxides (Pokrovsky et al., 2006). REE adsorption occurs primarily because imperfect substitution of elements into a mineral's crystal structure causes a negative surface charge (Coppin et al., 2002; Li and Zhou, 2020). Since LREE are more likely to exist as free species that can adsorb onto surfaces, they are more likely to be retained or even enriched in a profile. In contrast, the tendency of HREE to bond with colloids often results in HREE depletion in a profile.

Enrichment By Core/Profile

Fifty-two of the eighty-one cores and profiles analyzed using tau plots had at least one interval with REE enrichment. Of those, 50 show at least one interval of LREE enrichment, 36 show at least one interval of MREE enrichment, and 17 show at least one interval of HREE enrichment. The cores with the zones of greatest enrichment relative to the "parent" composition are as follows: 302-072 (up to 168%, unnamed coal; up to 150%, Upper Freeport), 230-092D (up to 131%, Little No. 5 Block Coal), 306-061 (up to 186%, Middle Kittanning), 282-026 (up to 106%, ~35' below Brush Creek Coal), 309-055 (up to 159%, ~10' below Middle Kittanning), KGSc334 (up to 206%, Hitchins), KGS546 (up to 1071%, WK6 Zone paleosol; up to 237%, Springfield paleosol; up to 145%, Tradewater Fm paleosol; up to 108%, Shelburn unnamed paleosol), IND063_2361 (up to 157%, Pottsville Fm), MD-4 (up to 153%, Mt. Savage claystone?), OGS-CSH0033 (up to 119%, Middle Mercer), OGS-CSH0062 (up to 375%, Clarion). As discussed previously, tau values were calculated relative to the least weathered sample and thus percent enrichment and depletion should be viewed as

estimates. Tau plots for all cores are given in **Appendix VI**.

Due to the higher mobility of HREE, they are believed to be less commonly enriched in the environment. However, tau plots have identified cores and profiles with intervals of significant HREE enrichment, which include but are not limited to KGSc334 (up to 138%, Hitchens), 306-061 (up to 157%, Middle Kittanning), 302-072 (up to 148%, claystone below unnamed coal), KGS 546 (up to 103%, Shelburn Formation unnamed paleosol; up to 195%, Springfield paleosol; up to 842%, WK6 zone paleosol), 230-092D (up to 131%, Below No. 5 Block Coal), and OGS-CSH0033 (up to 77%, Middle Mercer).

Enrichment By Unit

Thirty-nine of the units sampled by profiles and/or cores show at least some REE enrichment relative to the "parent" composition. Of those, 37 show LREE enrichment, 27 show MREE enrichment, 19 show HREE enrichment, and 10 show Y enrichment. LREE enrichment seems to be most common in study samples, with MREE enrichment also occurring regularly. HREE enrichment is less common, which is unsurprising given the higher mobility of HREE, however, it is still present in some of the units sampled.

The study does not have enough profiles from any given unit to draw statistically significant conclusions about REE enrichment in the unit as a whole. However, some preliminary observations can be made about the units sampled the most in the study. The Clarion (6 cores/profiles), Upper Kittanning (8 cores/ profiles) Middle Kittanning (18 cores/profiles), Lower Kittanning (12 cores/profiles), Upper Freeport (12 cores/profiles), and Lower Freeport (7 cores/profiles) were sampled in the largest number of cores and profiles. The Clarion shows REE enrichment in 17% of cores and profiles that it was sampled in; the Upper Kittanning had enrichment in 50% of cores and profiles, the Middle Kittanning had enrichment in 67% of cores and profiles, the Lower Kittanning had enrichment in 43% of cores and profiles, the Upper Freeport had enrichment in 75% of cores and profiles, and the Lower Freeport had enrichment in 57% of cores and profiles. Only one of the cores or profiles that sampled the Clarion underclay is REE enriched, however, it shows significant LREE and MREE enrichment, with a maximum enrichment of ~ 375% for La. Of the four enriched Upper Kittanning sections, all show LREE enrichment, while two show MREE and HREE enrichment. Y enrichment is not present in the cores sampled. Eleven of the enriched Middle Kittanning profiles show LREE enrichment, seven show MREE enrichment, and one shows HREE and Y enrichment. Of the five enriched Lower Kittanning sections, four exhibit LREE enrichment, one shows MREE enrichment, and one displays very slight (~2%) HREE enrichment. All nine of the enriched Upper Freeport sections show LREE enrichment, while 7 show MREE enrichment and three show at least slight HREE enrichment. None of the Upper Freeport sections exhibit Y enrichment. Of the four enriched Lower Freeport sections, three have LREE enrichment, two have MREE enrichment, and one has very slight (~4%) HREE enrichment. None of the sections show Y enrichment.

Mineralogic Influence on REE Enrichment

To determine what phases may be influencing REE enrichment, t_{Fe}, t_P, and t_{Al} were compared to τ values for REE. τ_{Fe} values are interpreted to reflect the abundance of iron oxides, both as crystalline minerals and amorphous phases. τ_{Al} values are interpreted to reflect the abundance of crystalline and amorphous aluminum-rich phases, such as kaolinite, gibbsite, and allophane, while τ_P values are interpreted to reflect the abundance of phosphates. These elements were chosen because phosphates are known to incorporate REE, while REE are known to adsorb onto aluminum-rich phases like kaolinite and in some cases Fe oxides.

Examples of iron oxide (τ_{Fe}), phosphate (τ_P), and Al-rich phases (τ_{Al}) controlling REE enrichment are shown in **Figures 8, 9, & 10**, respectively. Note how the tau pattern for Fe, P, or Al follows that of the LREE, MREE, and/or HREE, with areas of significant τ_{Fe}, τ_P, or τ_{Al} enrichment corresponding with REE enrichment, and areas of less τ_{Fe}, τ_P, or τ_{Al} enrichment or

depletion corresponding with REE depletion. In the six units which were sampled the most in this study, phosphates and/or Al-rich phases seem to be the primary controls on REE enrichment, with Fe locally influencing REE content. Phosphates seem to control REE in most of the zones of greatest enrichment, which are discussed above in the Enrichment by Core/Profile section. Fe oxides and Al-rich phases also appear to influence REE enrichment in some of the greatest enrichment zones, although their influence is less widespread in study samples than that of phosphates. Tau plots suggest Fe may play an important role in highly REE-enriched paleosols. There is not a clear mineralogical preference for LREE vs MREE vs HREE in the zones of greatest enrichment or in the most sampled units.

Mineralogic controls on REE distribution can be complex and vary with depth. Sometimes different enrichment peaks in the same section may be influenced by different mineralogic controls. For example, the clay unit located ~22 ft. below Brush Creek coal base in core 308-007 is shown in **Figure 11**. The tau plot suggests iron oxides (represented by τ_{Fe}) are the primary control on LREE enrichment around 299 ft. and 304 ft. depth. In contrast, phosphates (represented by τ_P) appear to control the MREE enrichment near 305 ft. depth, and the slight MREE enrichment around 301ft. Additionally, due to the complex processes that redistribute REE in the environment, a concentration of a particular mineral may cause REE enrichment at one depth in a core or profile, but not higher or lower in the section. For example, there is a spike in τ_P at around 297 ft. depth in **Figure 11**, and while MREE are less depleted at that depth than they are in areas with P depletion, they are not enriched relative to the "parent" composition. Furthermore, depths with the greatest enrichment of a mineral may not always correspond to greatest REE enrichment. In **Figure 11**, P is more enriched at 301 ft. than at 305 ft., whereas MREE are more enriched at 305 ft. than 301 ft. This means an interval significantly enriched in, for example, P may not always correlate with high REE concentrations; however, it may be worth screening the interval to confirm. Thus, high P and Al values, and in some circumstances Fe, may prove to be a first-order screening tool for REE in the Appalachian basin underclays.

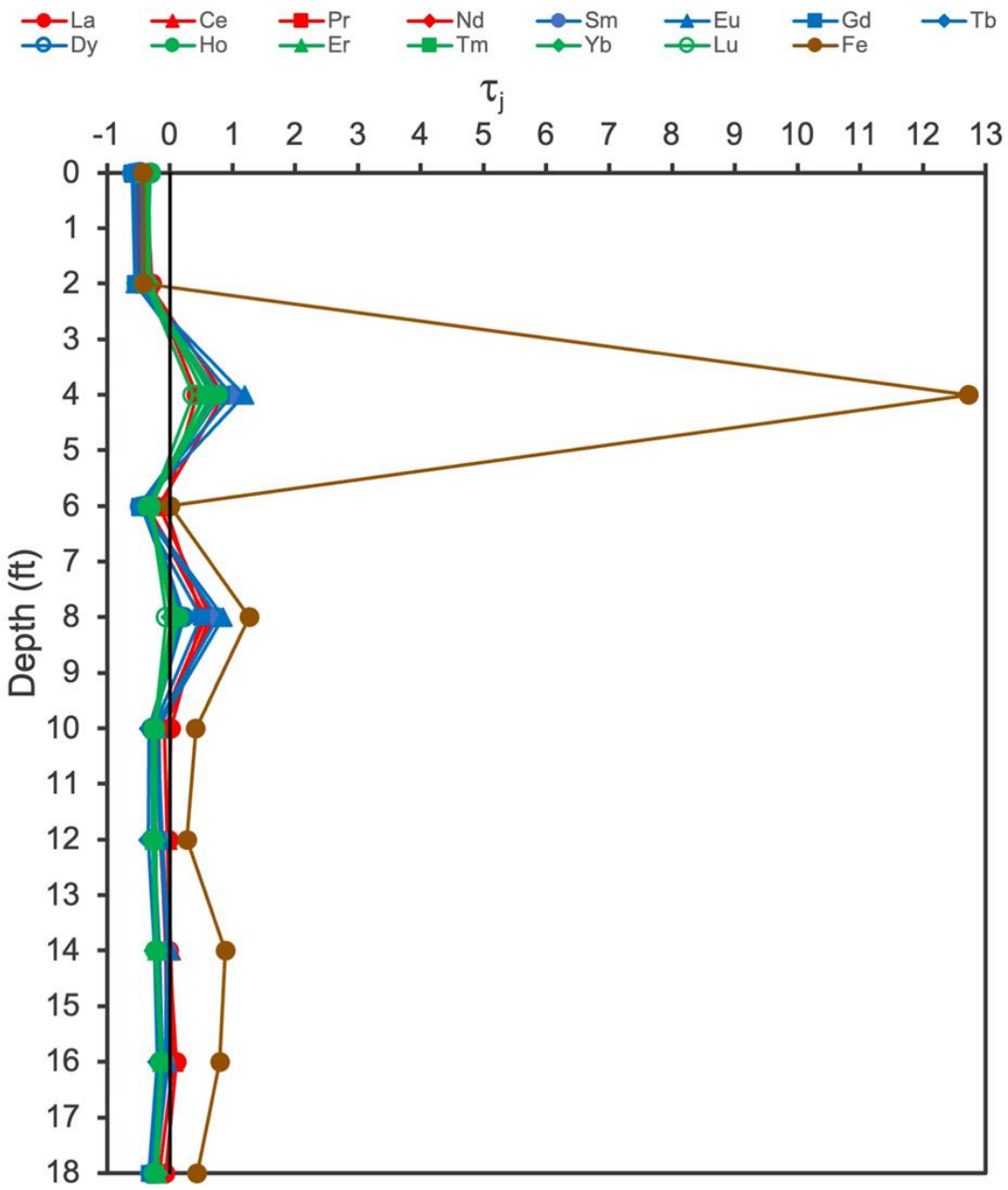

Figure 8. *Ohio Middle Mercer profile CSH0033 tau plot showing Fe oxides influencing REE retention. τ_j refers to the tau value for an element, j, shown in the legend. Solid black line at $\tau_{REE}=0$ denotes boundary between enrichment and depletion.*

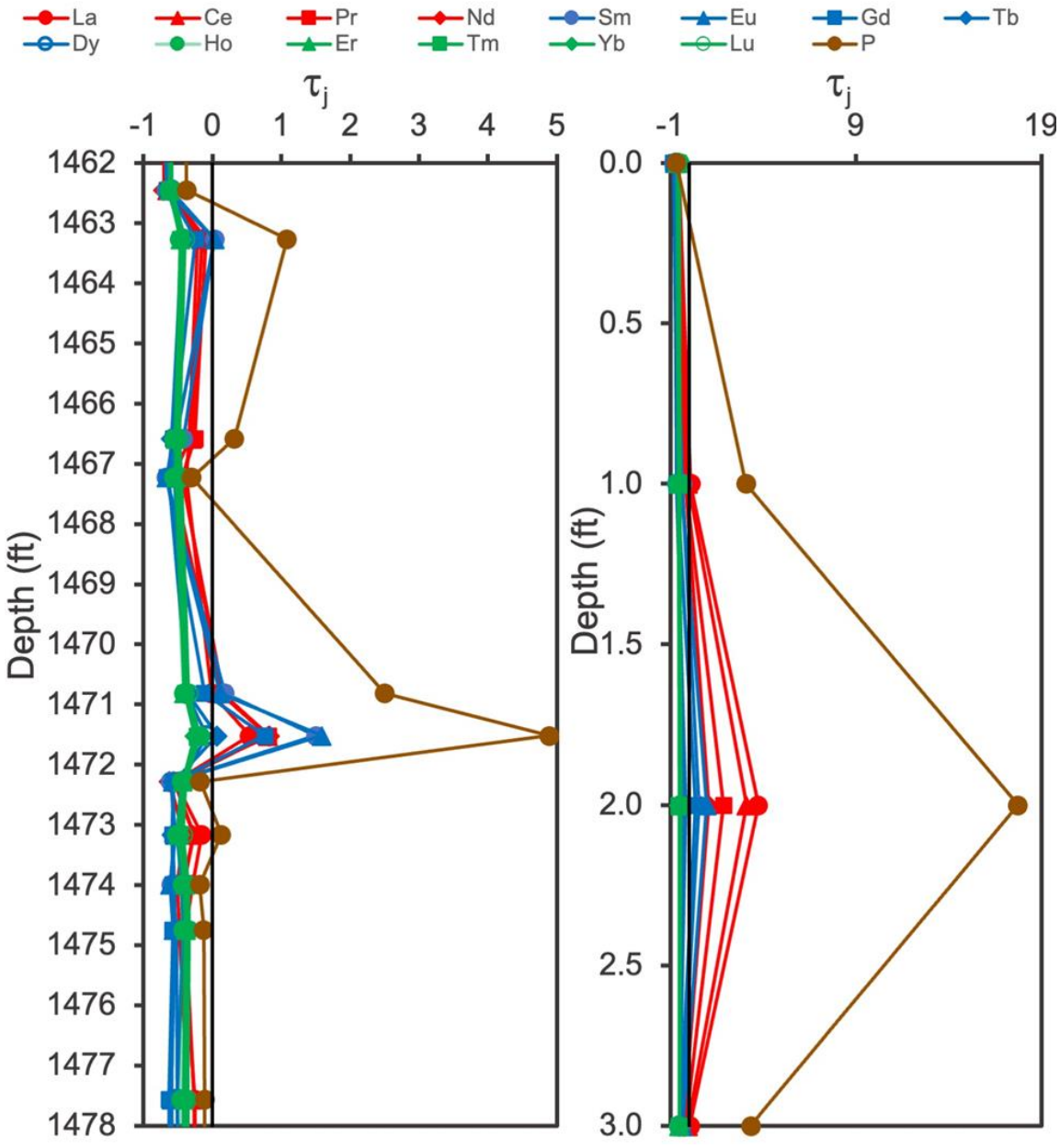

Figure 9. *Examples of underclay tau plots showing phosphates influencing REE retention. a. Middle Kittanning section of West Virginia core 309-055 and b. Ohio Clarion underclay profile CSH0062.* τ_j *refers to the tau value for an element, j, shown in the legend. Solid black line at* $\tau_{REE}=0$ *denotes boundary between enrichment and depletion.*

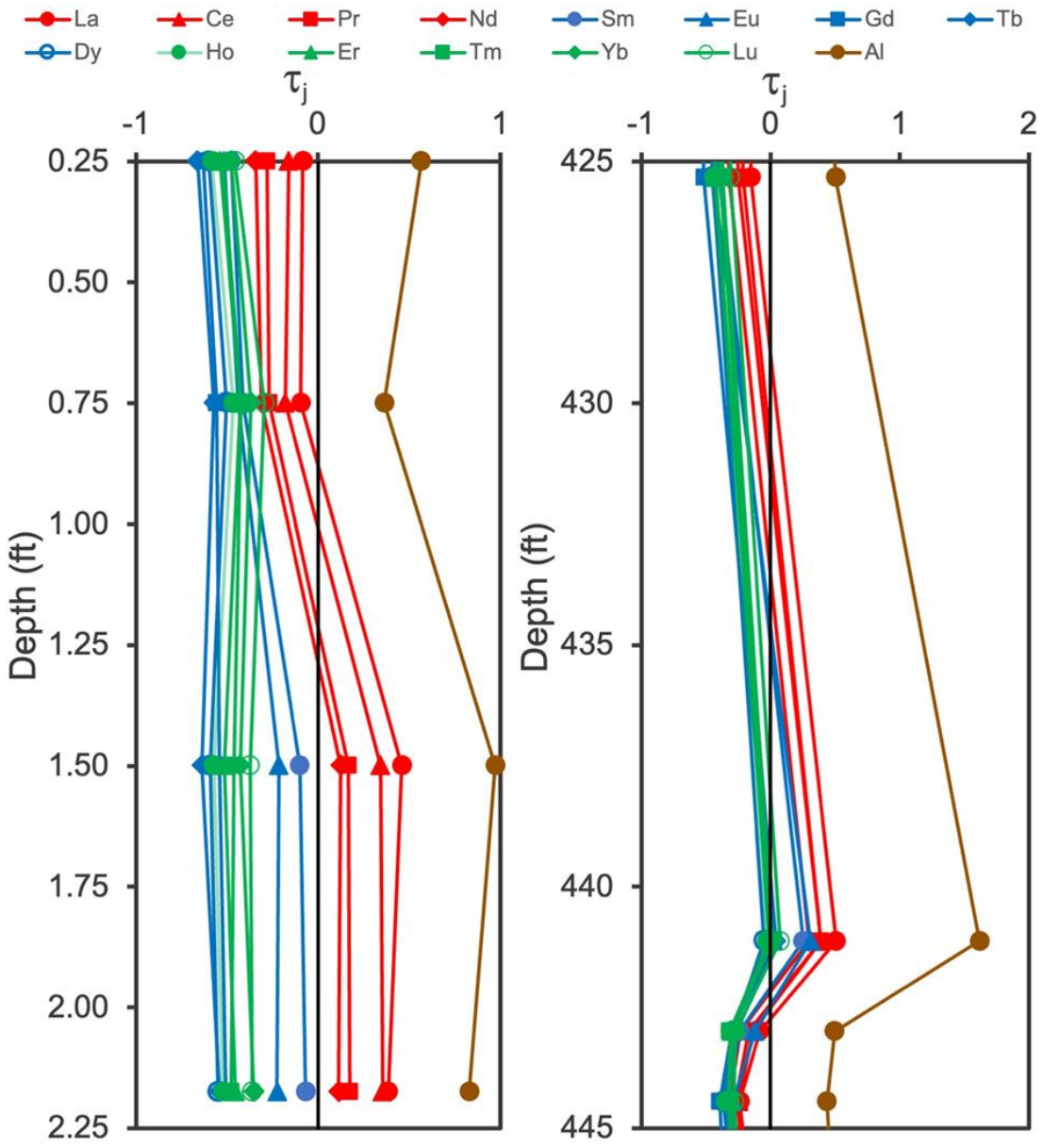

Figure 10. *Examples of underclay tau plots showing Al-rich phases influencing REE retention. a. Maryland Middle Kittanning profile MD-14B and b. Upper Kittanning section of West Virginia core 302-072.* τ_j *refers to the tau value for an element, j, shown in the legend. Solid black line at* $\tau_{REE}=0$ *denotes boundary between enrichment and depletion.*

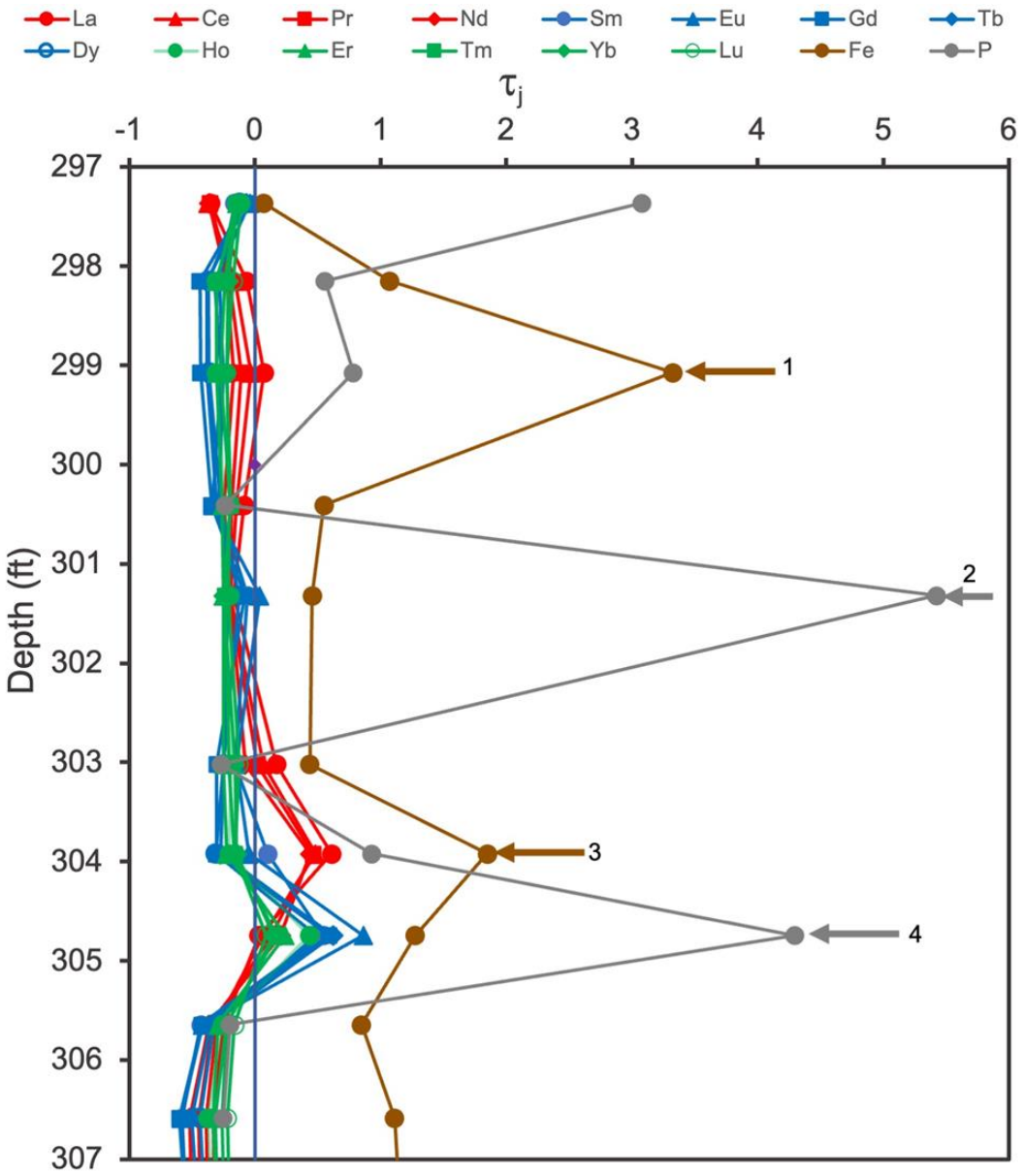

Figure 11. *Sample taken ~22 ft below Brush Creek coal base section in West Virginia core 308-007 showing multiple mineralogic influences on REE retention.* τ_j *refers to the tau value for an element, j, shown in the legend. Solid line at* $\tau_{REE}=0$ *denotes boundary between enrichment and depletion.*

REE Mobility in Cores and Profiles

All cores and profiles sampled in this study show significant evidence of REE mobility, however, the REE distribution that results from that mobility is due to locally occurring processes and thus varies with location for a given unit. In some cores and profiles, REE enrichment is seen near the base of a given unit while depletion is present at shallower depths. This occurs when REEs bond to colloids and other particles and are transported (translocated) downward by fluids. The REE eventually adsorb on to an existing mineral or amorphous phase, or are incorporated into a newly forming phase, causing enrichment. Examples of downward translocation can be seen in profiles MD-13 and the Upper Mercer section of core 306-061 (**Figure 12**). Downward translocation can also cause enrichment midway

down a unit, as seen in profile CSH0062 from the Clarion underclay (**Figure 13**). In some cases, enrichment occurs in the uppermost portion of a given core or profile, as seen in profile 230-092D, and the Shelburn Formation unnamed paleosol in core KGSc546 (**Figure 14**). This upper profile enrichment can result from the addition of REE from above, such as the downward translocation of REE from an overlying unit, or from biolifting, where roots draw nutrients upward from lower in a profile. Processes such as downward translocation and biolifting can redistribute REE in complex ways causing significant variability within a unit (**Figure 15**). Thus, when characterizing a unit for possible REE recovery, it is important to use a profile-based approach with an appropriate sampling interval.

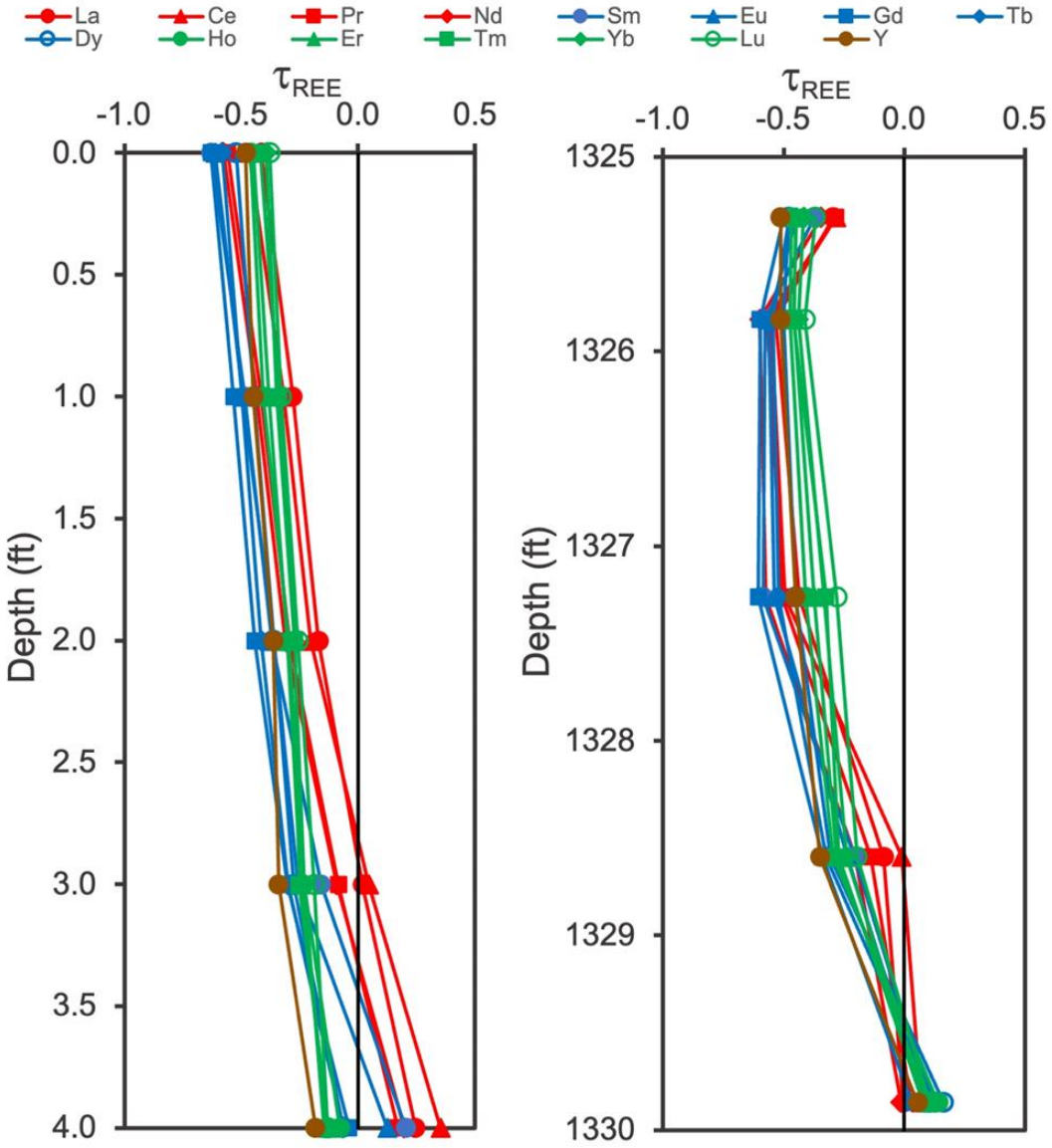

Figure 12. *Examples of tau plots showing enrichment at base of section due to downward translocation. a. Maryland Middle Kittanning profile MD-13 and b. Upper Mercer section of West Virginia core 306-061. Solid black line at* τ_{REE}*=0 denotes boundary between enrichment and depletion.*

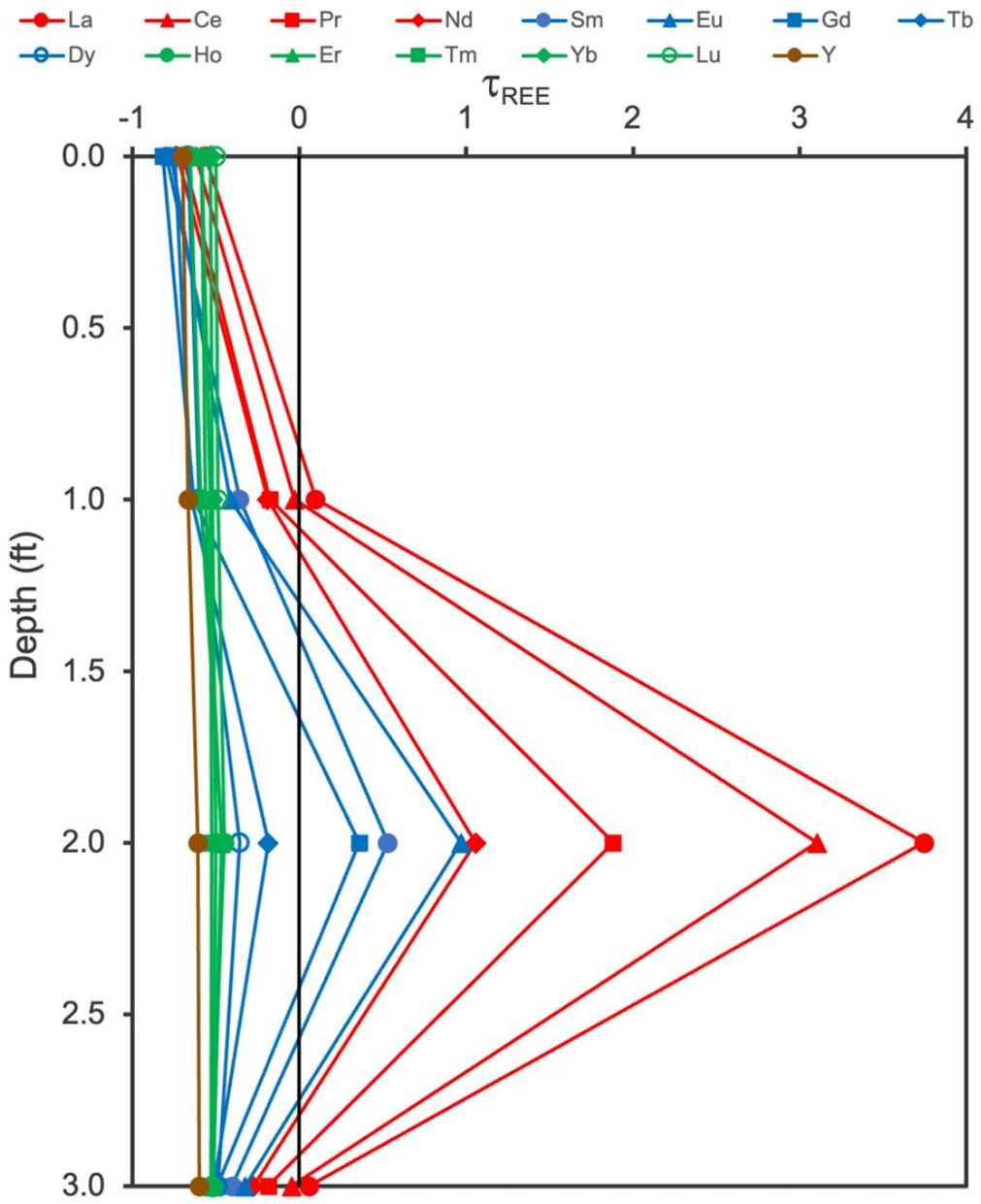

Figure 13. *Tau plot for Ohio Clarion underclay profile CSH0062 showing partial downward translocation. Solid black line at* $\tau_{REE}=0$ *denotes boundary between enrichment and depletion.*

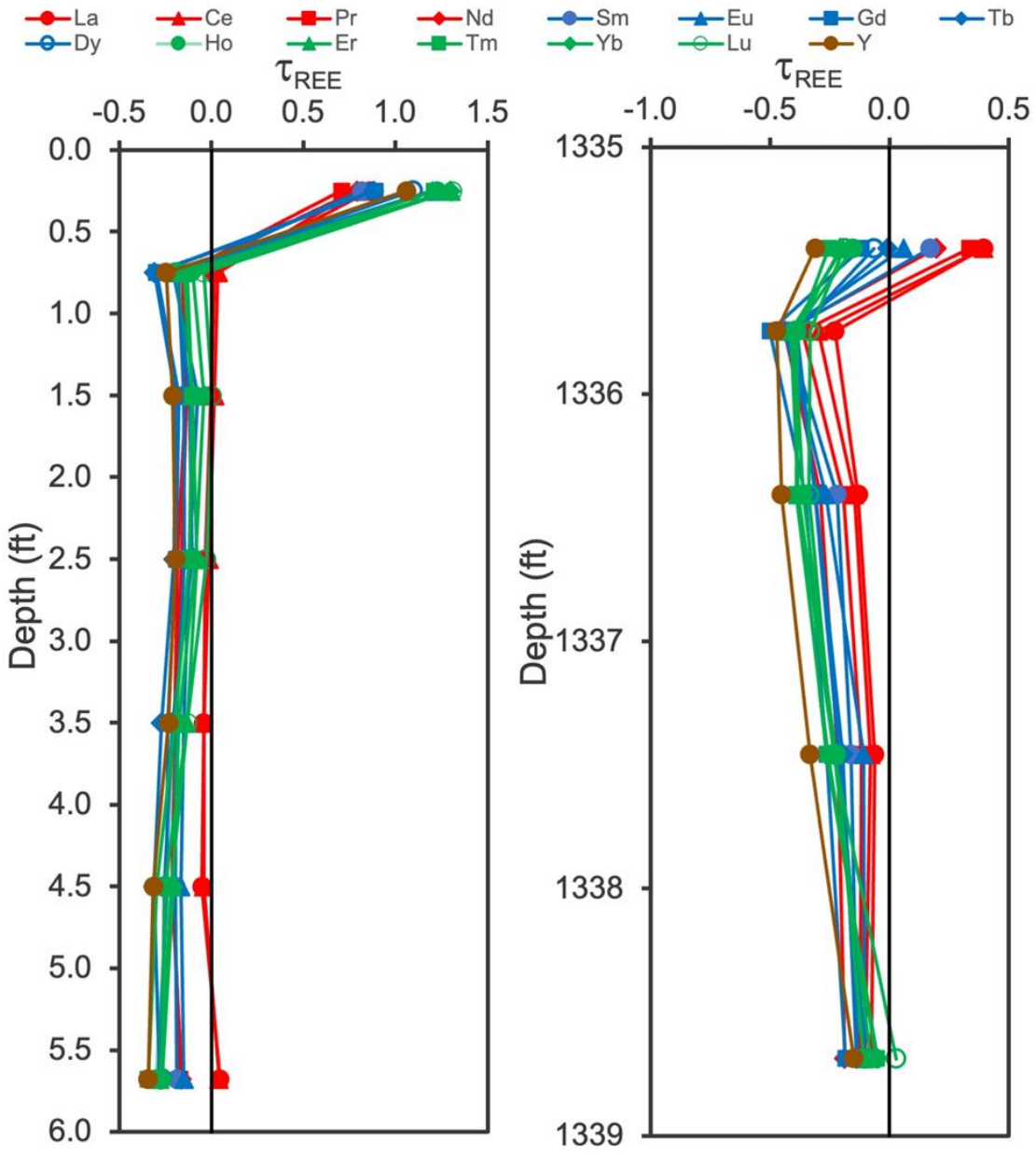

Figure 14. *Examples of underclay tau plots showing REE enrichment at the top of the section. a. West Virginia profile 230-092D (below No. 5 Block) and b. not named (Upper Mercer Coal) from West Virginia core 306-061. Solid black line at* $\tau_{REE}=0$ *denotes boundary between enrichment and depletion.*

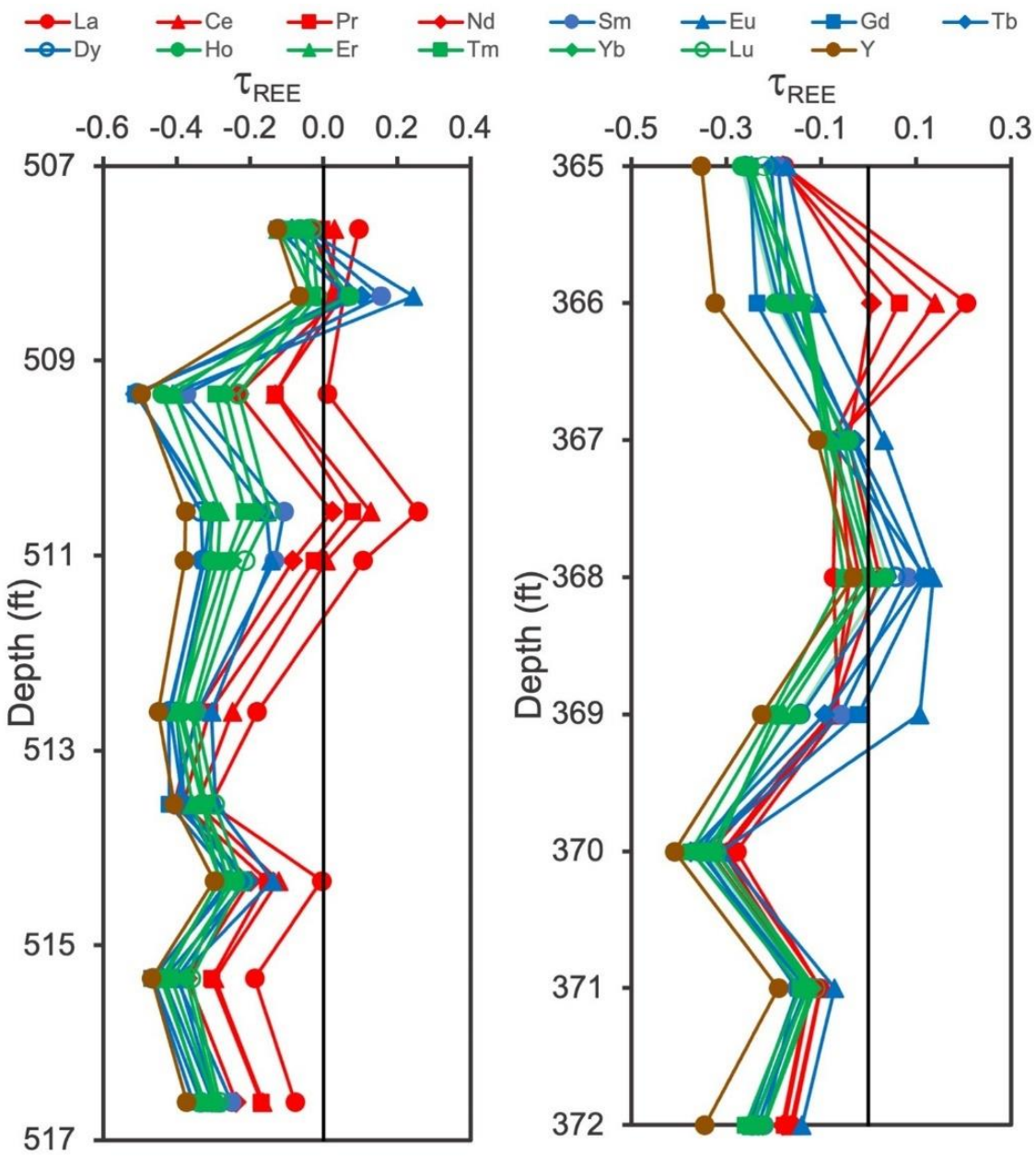

Figure 15. *REE mobility can produce complicated variability in REE enrichment and depletion. a. Upper Freeport section of West Virginia core 282-026 and b. Princess 5 paleosol section of Kentucky core KGSc334. Solid black line at* τ_{REE}*=0 denotes boundary between enrichment and depletion.*

Conclusions

A first-of-its-kind, multi-state geochemical reconnaissance study of Pennsylvanian claystones associated with coal horizons was conducted by workers from eight state geological surveys in cooperation with the USGS Earth MRI Program. Sampling parameters were broad and intended to be informed by institutional knowledge. A majority of samples were sourced from existing state-held collections due to unprecedented travel restrictions during the height of Covid-19 mandated lockdowns. Despite these limits on background information and sampling localities, results of the investigation showed REE enrichment above 300 ppm in nearly 20% of the samples analyzed (208 of 1062

samples, or 19.6%). Samples from the Appalachian basin were more commonly enriched; 180 of the 772 Appalachian basin samples had TREE concentrations greater than 300 ppm (23%), while only 9.7% of the 290 samples collected from Illinois basin underclays had greater than 300 ppm TREE (n=28). Two samples, one from Indiana and one from Ohio, had measured TREE concentrations greater than 1,200 ppm, constituting the highest values observed in the study.

Association of REEs with Al, P, Fe, and Sr is indicated by results from multiple analytical techniques combined with data analysis via machine learning, principal component analysis, and tau plots. Mineralogical analysis via XRD confirms that kaolinite is the dominant clay mineral present and that common REE-associated minerals such as monazite, xenotime, and bastnaesite are absent, suggesting that the REEs are not contained within certain minerals but are free throughout clays. Other critical minerals of interest, such as lithium, gallium, and indium, are present in varying amounts but do not appear to be enriched across the study area. Lithium and gallium are present in nearly all the samples. The highest lithium concentration observed is 1,100 ppm in a sample taken from Lawrence County, PA. Gallium is concentrated above crustal abundance of 19 ppm in 88% of the samples. Indium is only observed in 20 samples across the region.

Intervals of REE enrichment are present in 52 of the 81 cores and profiles sampled. While LREE enrichment is the most common, MREE and HREE enrichment are also noted. In the six units which were most densely sampled, phosphates and/or Al-rich phases seem to be the primary controls on REE enrichment, with Fe locally influencing REE content. Phosphates appear to control REE in most of the zones of greatest enrichment, with Fe-oxides and Al-rich phases exerting less widespread influence and Fe potentially playing an important role in highly REE-enriched paleosols. Significant evidence of REE mobility is observed in all cores and profiles. Processes such as biolifting and downward translocation cause an uneven vertical distribution of REE in units, necessitating a profile-based approach with appropriate sampling intervals to adequately characterize REE enrichment and depletion in a given location.

Data obtained through this Earth MRI study provides valuable information on the distribution of REEs in the Appalachian and Illinois basins. More in-depth studies are required to understand the abundance and extent of these critical mineral zones.

Acknowledgements

The authors thank all of our colleagues at WVGES for their contributions and support, both directly and indirectly, to this study. This project was funded through the National Cooperative Geologic Mapping Program of the U.S. Geological Survey, grant award number G20AC00164WV. We are grateful to all the state surveys and their cooperation, all the contributors to the WV geochemical database, and to KGS for the coordination of the Illinois Basin. Also, a special thank you to Warren Day and everyone else at the USGS for guidance and access to information.

In addition, the authors are truly grateful for peer reviewers Ronald McDowell (WVGES), Bill Grady (retired WVGES), and Peter Rozelle (retired DOE) whose comments and suggestions were extremely helpful.

Contributors to this project from the state surveys include Aaron Bierley, Dave Brezinski, Jim Britton, Ryan Clark, Phil, Dinterman, Scott Elrick, Jared Freiburg, Frank Fugitt, Kristen Hand, Frank Fugitt, Kristen Hand, Will Junkin, Rebecca Kavage Adams, Gina Lukoczki, Maria Mastalerz, Pat McLaughlin, Richard Ortt, Stephane Tassier-Surine, Randy Toth, Derek Spurgeon, and JD Stucker. From the USGS; Jamie Azain, Bill Benzel, Warren Day, Connie Dicken, Jane Hammarstrom, Andrew Ingraham, and Steven Smith. And from NETL; Christopher Creason, Devin Justman, Scott Montross, Kelly Rose, and Thomas Tarka.

References

Anderson, S. P., Dietrich, W. E., and Brimhall, G. H. (2002). Weathering profiles, mass-balance analysis, and rates of solute loss: Linkages between weathering and erosion in a small, steep catchment. Bull. Geol. Soc. Am. 114, 1143–1158. doi:10.1130/0016-7606(2002)114<1143:WPMBAA>2.0.CO.

Babechuk, M. G., Widdowson, M., and Kamber, B. S. (2014). Quantifying chemical weathering intensity and trace element release from two contrasting basalt profiles, Deccan Traps, India. Chem. Geol. 363, 56–75. doi:10.1016/j.chemgeo.2013.10.027.

Bao, Z.W., and Zhao, Z.H., 2008. Geochemistry of mineralization with exchangeable REY in the weathering crusts of granitic rocks in South China. Ore Geology Reviews, v. 33, p. 519-535. https://doi.org/10.1016/j.oregeorev.2007.03.005

Beuthin, J.D., 1997. Paleopedological evidence for a eustatic Mississippian-Pennsylvanian (mid-Carboniferous) unconformity in southern West Virginia: Southeastern Geology, v. 37, p. 25-37.

Blake, B. M., Jr. and Beuthin, J. D., 2008. Deciphering the Mid-Carboniferous Eustatic Event in the Central Appalachian Foreland Basin, Southern West Virginia (USA). In: C. R. Fielding, T. D. Frank and J. L. Isbell (Editors), Resolving the Late Paleozoic Ice Age in Time and Space. Boulder, CO., Geological Society of America Special Paper 441, p.249-260.

Boynton, W.V. (1984) Cosmochemistry of the Rare Earth Elements: Meteorite Studies. In: Henderson, P., Ed., Rare Earth Element Geochemistry, Elsevier, New York, 63-114. https;//doi.org/10.1016/B978-0-444-42148-7.50008-3

Brezinski, D.K., and Kollar, A.D., 2011. Appalachian Pennsylvanian climatic events and their congruent biotic responses, in Ruffolo, R.M., and Ciampaglio, C.N., eds., From the Shield to the Sea: Geological Field Trips from the 2011 Joint Meeting of the GSA Northeastern and North-Central Sections: Geological Society of America Field Guide 20, p. 45–60, doi:10.1130/2011.0020(03).

Brimhall, G. H., and Dietrich, W. E. (1987). Constitutive mass balance relations between chemical composition, volume, density, porosity, and strain in metasomatic hydrochemical systems: Results on weathering and pedogenesis. Geochim. Cosmochim. Acta 51, 567–587. doi:10.1016/0016-7037(87)90070-6.

Bryan, R.C., Richers, D., Andersen, H.T., Gray, T., 2015. Assessment of Rare Earth Elemental Contents in Select United States Coal Basins. Document No: 114-910178X-100-REP-R001-00. Final report as prepared by Tetra Tech

Cantrell, K. J., and Byrne, R. H. (1987). Rare earth element complexation by carbonate and oxalate ions. Geochim. Cosmochim. Acta 51, 597–605. doi:10.1016/0016-7037(87)90072-X.

Cecil, C.B., Brezinski, D.K., Dulong, F., 2004. The Paleozoic record of changes in global climate and sea level: central Appalachian Basin. In: Southworth, S., Burton, W. (Eds.) U.S. Geol. Survey Circular 1264, p. 77–135.

Chadwick, O. A., Brimhall, G. H., and Hendricks, D. M. (1990). From a black to a gray box - a mass balance interpretation of pedogenesis. Geomorphology 3, 369–390. doi:10.1016/0169-555X(90)90012-F.

Conley, J.E., Brown, R.A., Cservenyak, F.J., Anderberg R.C., Kandiner, H.J., Green, S.J., 1947, Production of Metallurgical Alumina from Pennsylvania Nodular Diaspore Clays. Bureau of Mines B 465, 193p.

Coppin, F., Berger, G., Bauer, A., Castet, S., and Loubet, M. (2002). Sorption of lanthanides on smectite and kaolinite. Chem. Geol. 182, 57–68. doi:10.1016/S0009-2541(01)00283-2.

Eberl, D.D., 2003. User's Guide to Rockjock - A Program for Determining Quantitative Mineralogy from Powder X-Ray Diffraction Data, United States Geological Survey Open-File Report 2003-78, United States Geological Survey, Boulder, CO, 47p. https://doi.org/10.3133/ofr200378

Eggleston, J.R., 1996. History of West Virginia Mineral Industry-Clay. West Virginia Geological Survey Education Page, www.wvgs.wvnet.edu/www/geology/geoldvcl.htm.

Foley, N.K., Jaskula, B.W., Kimball, B.E., and Schulte, R.F., 2017, Gallium, chap. H of Schulz, K.J., DeYoung, J.H., Jr., Seal, R.R., II, and

Bradley, D.C., eds., Critical mineral resources of the United States—Economic and environmental geology and prospects for future supply: U.S. Geological Survey Professional Paper 1802, p. H1– H35, https://doi.org/10.3133/pp1802H.

Fortier, S.M., Nassar, N.T., Lederer, G.W., Brainard, Jamie, Gambogi, Joseph, and McCullough, E.A., 2018. Draft critical mineral list—Summary of methodology and background information—U.S. Geological Survey technical input document in response to Secretarial Order No. 3359: U.S. Geological Survey Open-File Report 2018–1021, 15 p., https://doi.org/10.3133/ofr20181021.

Hill, I. G., Worden, R. H., and Meighan, I. G. (2000). Yttrium: The immobility-mobility transition during basaltic weathering. Geology 28, 923–926. doi:10.1130/0091-7613(2000)28<923:YTITDB>2.0.CO;2.

Hofstra, A.H., and Kreiner, D.C., 2020, Systems-Deposits-Commodities-Critical Minerals Table for the Earth Mapping Resources Initiative (ver. 1.1, May 2021): U.S. Geological Survey Open-File Report 2020–1042, 26 p., https://doi.org/10.3133/ofr20201042.

Keller, W.D., Westcott, J.F., Bledsoe, A.O., 1953. The origin of Missouri fire clays: Clays Clay Miner. 2 (Second National Conference on Clays and Clay Minerals, University of Missouri), 7-46. https://doi.org/10.1346/CCMN.1953.0020104.

Kurtz, A. C., Derry, L. A., Chadwick, O. A., and Alfano, M. J. (2000). Refractory element mobility in volcanic soils. Geology 28, 683–686. doi:10.1130/0091-7613(2000)028<0683:REMIVS>2.3.CO;2.

Kurtz, A. C., Derry, L. A., and Chadwick, O. A. (2001). Accretion of Asian dust to Hawaiian soils: Isotopic, elemental, and mineral mass balances. Geochim. Cosmochim. Acta 65, 1971–1983. doi:10.1016/S0016-7037(01)00575-0.

Kynicky, J., Smith, M.P., and Xu, Cheng, 2012. Diversity of rare earth deposits: The key example of China. Elements, v. 8, p. 361–367. https://doi.org/10.2113/gselements.8.5.361

Laveuf, C., and Cornu, S. (2009). A review on the potentiality of Rare Earth Elements to trace pedogenetic processes. Geoderma 154, 1–12. doi:10.1016/j.geoderma.2009.10.002.

Li, M. Y. H., and Zhou, M. F. (2020). The role of clay minerals in formation of the regolith-hosted heavy rare earth element deposits. Am. Mineral. 105, 92–108. doi:10.2138/am-2020-7061.

Ma, L., Jin, L., and Brantley, S. L. (2011). How mineralogy and slope aspect affect REE release and fractionation during shale weathering in the Susquehanna/Shale Hills Critical Zone Observatory. Chem. Geol. 290, 31–49. doi:10.1016/j.chemgeo.2011.08.013.

Nesbitt, H. W., and Young, G. M. (1982). Early Proterozoic climates and plate motions inferred from major element chemistry of lutites. Nature 299, 715–717. https://doi.org/10.1038/299715a0

Patterson, S.H., Hosterman, J.W., 1958. Geology of the clay deposits in the Olive Hill District, Kentucky: Clays Clay Miner. 7 (Proceedings of the Seventh National Conference on Clays and Clay Minerals), 178-194. https://doi.org/10.1016/B978-08-009235-5.50014-0.

Pokrovsky, O. S., Schott, J., and Dupré, B. (2006). Trace element fractionation and transport in boreal rivers and soil porewaters of permafrost-dominated basaltic terrain in Central Siberia. Geochim. Cosmochim. Acta 70, 3239–3260. https://doi.org/10.1016/j.gca.2006.04.008.

Rozelle, P.L., Khadilkar, A.B., Nuerxida, P., Soundarrajan, N., Klima, M.S., Mosser, M.M., Miller, C.E., Pisupati, S.V., 2016. A study on removal of rare earth elements from U.S. coal by-products by ion exchange. Metallurical and Materials Transactions, E 3(1), 6-17. https://doi.org/10.1007/s40553-015-0064-7.

Rygel, M.C., and Beuthin, J. D., 2002. Paleopedology of a residual clay associated with the Mississippian-Pennsylvanian (MID-Carboniferous) unconformity, southwestern Pennsylvania. Southeastern Geology, v. 41, no. 3, p. 129-143.

TetraTech, Inc., 2018. Identification and characterization of coal and coal by-products containing high Rare Earth Element concentrations. Final Report, U.S. Department of Energy contract # DE-FE-00266478. URL: https://edx.netl.doe.gov/ree/?page_id=2169

Tourtelot, H.A. and Brenner-Tourtelot, E.F. (1977). Lithium, a preliminary survey of its mineral occurrence in flint clay and related rock types in the United States a preliminary survey. U.S. Geological Survey Open File Report, 77-786, 50 p., doi:10.3133/ofr77786

Tyler, G. (2004). Rare earth elements in soil and plant systems - A review. Plant Soil 267, 191–206. doi:10.1007/s11104-005-4888-2.

Van Gosen, B.S., Verplanck, P.L., Seal, R.R., II, Long, K.R., and Gambogi, Joseph, 2017, Rare-earth elements, chap. O *of* Schulz, K.J., DeYoung, J.H., Jr., Seal, R.R., II, and Bradley, D.C., eds., Critical mineral resources of the United States—Economic and environmental geology and prospects for future supply: U.S. Geological Survey Professional Paper 1802, p. O1–O31, https://doi.org/10.3133/pp1802O.

Williams, E.G., 1960. Relationship between the stratigraphy and petrography of Pottsville sandstones and the occurrence of high-alumina Mercer Clay: Econ. Geol. 55(6), 1291-1302. https://doi.org/10.2113/gsecongeo.55.6.1291.

Williams, E.G., Bragonier, W.A., 1974. Controls of Early Pennsylvanian sedimentation in western Pennsylvania. In: Briggs, G. (Ed.), Carboniferous of the Southeastern United States, Geological Society of America, Special Paper 148. Geological Society of America, Inc., Boulder, CO, pp. 135-152. https://doi.org/10.1130/SPE148-p135

Williams, E.G., Bragonier, W., 1985. Origin of the Mercer high-alumina clay. In: Gold, D.P. (Ed.), 50th Annual Field Conference of Pennsylvania Geologists: Central Pennsylvania Geology Revisited, October 4, 5, and 6, 1985. Field Conference of Pennsylvania Geologists, Harrisburg, PA, pp. 204-211.

Appendix

Appendices can be viewed and downloaded at https://downloads.wvgs.wvnet.edu/pubcat/docs/RI37_Appendices.pdf

Appendix I. WVGES Core Photos, Loggers Reports, Strater Logs, and a First Round Sampling Report

Appendix II. Orange Methodology and data

Appendix III. USGS Format of all Location, ICP-OES-MS & WDXRF Data

Appendix IV. hhXRF Data

Appendix V. XRD Data

Appendix VI. Tau Plots